Promoting Modes and Demoting Modes in Enzyme-Catalyzed Proton Transfer Reactions: A Study of Models and Realistic Systems

Qiang Cui*,[†,‡] and Martin Karplus*,[†,§]

Department of Chemistry and Chemical Biology, Harvard University, Cambridge, Massachusetts 02138, Department of Chemistry and Theoretical Chemistry Institute, University of Wisconsin, Madison, 1101 University Avenue, Madison, Wisconsin 53706, and Laboratoire de Chimie Biophysique, ISIS Universitè Loius Pasteur, 67000 Strasbourg, France

A number of proton transfer reactions have been studied to reveal the identity of modes that influence the rate constant, especially in the context of enzyme catalysis. Results with analytic model potentials confirmed the general notion that the effect of a given mode on the proton transfer rate depends on the symmetry of its coupling with the proton transfer coordinate. Symmetrically coupled modes have promoting effects at both high and low temperatures, although the origin of promotion is largely *classical* at room temperature and the increase of tunneling is important only at low temperature. Antisymmetric modes have "demoting effects" mainly because the antisymmetric coupling gives rise to asymmetry in the effective potential along the proton transfer coordinate and therefore restricts tunneling to occur effectively only when the mode is vibrationally excited. Thus, vibrational excitation of both types of modes can be important for the proton transfer rate. Calculations on TIM with a QM/MM potential clearly demonstrated that the proton transfer is strongly coupled to a large number of vibrations (including both symmetric and antisymmetric modes), which in general are localized to atoms in the active site. One of the modes is the donor−acceptor stretch, which modulates the effective barrier for the proton transfer and also the effect of tunneling. There are also other modes that are symmetrically or antisymmetrically coupled to the proton-transfer coordinate, and they involve nearby residues such as Ala 212 and Ile 170. Their effect is to adjust the enzyme environment by lowering the effective proton-transfer barrier. We propose procedures to identify motions that are important for the proton transfer based on reaction path curvature and coupling coefficients. We also emphasize that the minimum energy path (MEP) involves changes in environmental variables, such as the donor−acceptor stretch, as the primary part in the reactant and product regions and includes significant proton motion only near the barrier. Thus, there is no fundamental conflict between the MEP description of proton transfers at room temperature and Marcus type of models in the adiabatic regime; that is, both include contributions from change in the zero-point energies.

I. Introduction

Understanding how enzymes achieve their remarkable catalytic efficiencies has been one of the most challenging and exciting endeavors in biochemistry. Over the past several decades, different proposals have been put forward to explain the origin of catalysis in a large number of enzymes;[1] the list of mechanisms include electrostatic polarization or stress,[2] reduced reorganization energy,[3] entropic effects,[4] low-barrier hydrogen bonds,[5] etc. All of those fall in the class of mechanisms that lower the free energy barrier, either by ground-state destabilization, transition-state stabilization, or both. One other factor that has been discussed for a long time,[6] but without specific analysis, concerns enzyme dynamics,[7,8] i.e., the idea that the internal motions of enzymes have a direct role in catalysis.[9] Recently, this general proposal has been employed to explain certain aspects of enzyme catalysis of proton (hydride) transfer. It has been recognized that the height and width of the barrier for such reactions are sensitive to the donor−acceptor distance, and it is conceivable, therefore, that donor−acceptor vibrational dynamics has a strong influence on the rates of proton (hydride) transfers. It has been proposed also that the tunneling coefficient for proton/hydride transfer is a sensitive function of the donor−acceptor distance, which makes the influence of donor−acceptor dynamics of even greater interest.[10] In addition, for reactions in condensed media, including enzymes, the role of the solvent (protein environment) has been stressed,[10,11,23,64] and it has been suggested that additional coordinate, "perpendicular" to the reaction coordinate, can be used to include this effect. In such descriptions, the instantaneous structure of the solvent plays an essential role in determining whether a reaction takes place.

Evidence in support of the role of dynamics in proton (hydride) transfer and tunneling has come largely from the kinetic studies of Klinman and co-workers,[12] although others have contributed as well.[13] Kinetic isotope effects (KIE) and their temperature dependence have been measured for a number of enzymes, including alcohol dehydrogenases,[14] amine oxidases,[15] glucose oxidases,[16] and lipoxygenase.[17] Particularly interesting is a recent study of a thermophillic alcohol dehydrogenase from *Bacillus stearothermophilus*,[14a] whose optimum

temperature is 65 °C. Measured KIEs were interpreted as suggesting a significant tunneling contribution between 30 and 65 °C but considerably less tunneling at temperatures in the range of 5−30 °C. Such a counterintuitive result was rationalized by the suggestion that the thermophillic enzyme becomes more rigid at lower temperature[18] and that, therefore, certain modes that are essential for tunneling (e.g., modes changing the donor−acceptor distance) are no longer excited. In glucose oxidase (GO),[16] different GO glycoforms (with about 8, 120, and 400 bound sugars, respectively) were investigated, and it was suggested that the contribution from tunneling is the largest in the least glocosylated enzyme. The variation in tunneling was characterized by the D/T isotope effect on the Arrhenius preexponential factors, which were 0.89 ± 0.04, 1.30 ± 0.10, and 1.47 ± 0.09 for three GO glycoforms in the order of decreasing glycosylation; a larger D/T Arrhenius prefactor correlates with a larger magnitude of tunneling.[12] This was rationalized by the fact that glycosylation can induce protein rigidity,[19] although no quantitative analysis was provided. The two examples we have cited are not the only ones,[12,13] but they have played an important role in focusing attention[7] on the possible role of protein dynamics in determining the extent of tunneling and, more generally, on the importance of tunneling in enzyme catalysis. This being said, there is no direct evidence that dynamics plays a dominant role in the enzymatic rate acceleration, which can be as large as 10^{17}, relative to the reaction in solution.[1]

In recent theoretical analyses,[20,25] efforts were made to determine the identity of the vibrational modes in proteins that can strongly influence the rate of proton transfer. Most discussions have focused on so-called "promoting modes", whose excitation increases the rate of reaction. However, as we will demonstrate, there are also modes, which we call "demoting modes", whose presence decreases the rate. Based on earlier work on small (two-dimensional) gas-phase models by Bendenskii and co-workers[21] with the instanton approach,[22] it was argued that the effect of the modes coupled to the proton-transfer coordinate depends on the symmetry of the coupling. If the mode is *symmetrically* coupled to the proton-transfer coordinate (i.e., the mode has displacements of the same sign in the reactant and product relative to the saddle point; see Figure 2 for an illustration), the proton-transfer rate is increased relative to the reaction without the coupling (i.e., the mode has a "promoting effect"), because the effective proton-transfer barrier is reduced as the mode Q is vibrationally excited. An often-discussed symmetric mode in proton transfer is the donor−acceptor stretching motion,[2,24,25] which was emphasized by Hynes and co-workers for reactions in solution, such as model proton transfer in CH_3Cl.[23] Their formulation highlights the importance of polarization by the solvent and of solute vibrations, rather than the potential barrier height along the proton coordinate, in determining the apparent activation free energy barrier. The donor−acceptor vibration ("promoting mode") was found to be crucial because it modulates, in an exponential fashion, the tunneling coupling matrix element.[23] In the nonadiabatic proton transfer regime (i.e., the ground energy level of the proton coordinate is lower than the potential barrier and the proton transfer is dominated by tunneling), it was assumed that tunneling occurs only through the ground vibrational state along the proton transfer coordinate (an assumption which is valid only at low temperatures), and a perturbative treatment was used for the tunneling matrix element.[23] In the adiabatic proton-transfer regime (i.e., the ground energy level of the proton coordinate is higher than the potential barrier and thus no

tunneling is involved), the recent analysis by Kiefer and Hynes,[26] published while this paper was being reviewed, also found that the donor−acceptor vibration makes a substantial contribution to the free energy barrier. The interaction with the environment (solvent, protein) can be described approximately by a mode that is *antisymmetrically* coupled to the proton-transfer coordinate (see Figure 3).[27] This corresponds to the fact the solvent molecules tend to reorganize (which causes a change in the solvent polarization potential) after the proton transfer because of the change in the charge distribution of the solute. In a mathematical model, this reorganization is represented by the different signs for the equilibrium value of the solvent coordinate before and after the reaction; that is, the solvent structure around the reacting moieties changes during the reaction. In the commonly used Kramers' type models for solvation effects,[28−31] the antisymmetric form of coupling is usually adopted. The tunneling effect is diminished relative to the reaction in the absence of the coupling in such a mode since an extra Franck− Condon penalty has to be paid because of the reorganization before and after the reaction (similar to electron-transfer reactions[36]); that is, proton tunneling can only occur effectively when the "solvent" degree of freedom is vibrationally excited in both the reactant and product; otherwise there is strong asymmetry in the effective proton-transfer potential that makes tunneling inefficient (e.g., see section III.1). For example, Schwartz and co-workers[25] used a two-dimensional solute Hamiltonian (proton transfer plus a symmetrically coupled mode) in the presence of bath modes represented by bilinearly (i.e., antisymmetrically) coupled harmonic oscillators. They emphasized the important contribution from vibrationally excited states and activated transfer over the barrier at finite temperatures. The symmetrically coupled mode still enhances the rate, although the effect is somewhat quenched by the presence of the bath.

Most previous studies, such as the ones cited above, have been restricted to model potentials; for example, a one-dimensional double-well potential with a bilinearly (i.e., antisymmetrically) or symmetrically coupled harmonic bath were used in refs 21 and 23−25. Because tunneling is very sensitive to the shape and height of the barrier, studies with a more realistic description of the potential energy surface are required to determine the importance of the various effects in real systems. In the current work, we carry out rate constant calculations including tunneling for a number of proton-transfer reactions involving both simple model systems (i.e., 2D and 3D analytical potentials and a small enediolate molecule in the gas phase) and a realistic system (i.e., proton transfer in the enzyme triosephosphate isomerase). Specifically, we examine the effect of modes coupled to the proton-transfer coordinate to determine if there are "promoting modes", and if so, what are their identities. We focus on the donor−acceptor vibration as the promoting mode because it is most likely to play a role and thus has been discussed by others. However, we also consider the possibility that other modes are important in the proton-transfer process; i.e., antisymmetric modes that undergo significant reorganization during the proton transfers. The problems for study were chosen such that the semiclassical VTST method[32] (see the Computational Models section) is expected to be accurate, based on previous comparisons with rigorous quantum mechanical scattering calculations.[33,48,49] The model problems allow us to make clear the meaning of promoting modes and also to compare the VTST approach with other methods (primarily the Marcus model, see below) that have been used in the analysis of promoting modes.[23,25,26] We
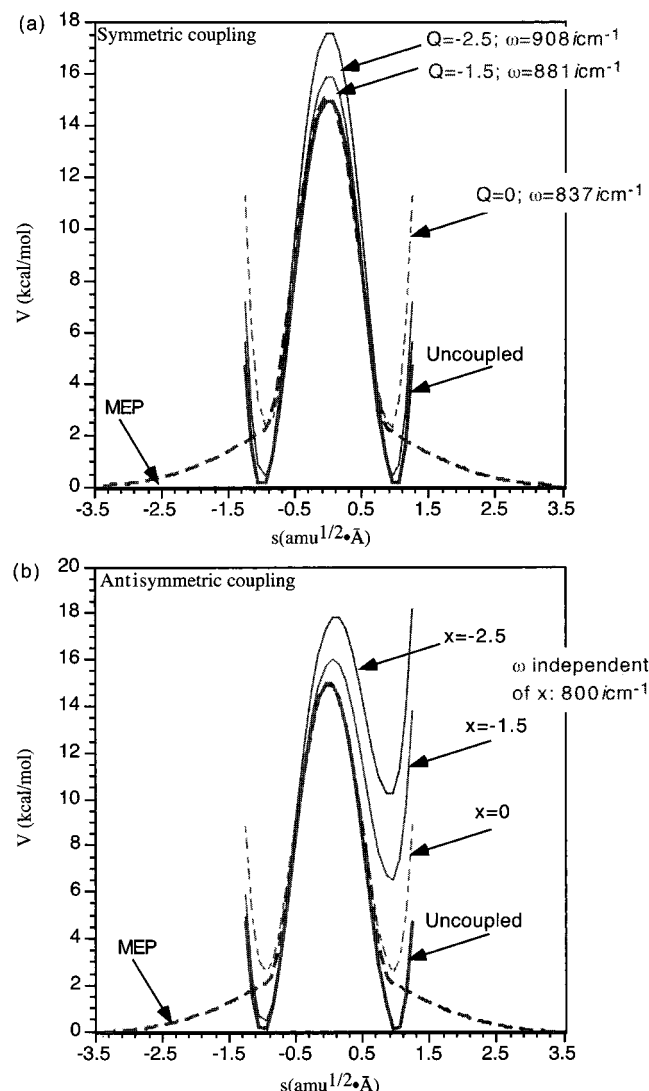
Enzyme-Catalyzed Proton Transfer Reactions

J. Phys. Chem. B, Vol. 106, No. 32, 2002 **7929**

Figure 1. One-dimensional effective potential along the proton-transfer coordinate (q) at fixed symmetrically coupled Q (a) or antisymmetrically coupled x (b) coordinate. Also shown are the uncoupled 1D potential and the energy along the minimum energy paths. For the form of the potentials, see eqs 1 and 2, and see Table 1 for the parameters used. Note the difference in the effective barrier frequencies in different cases.

study the first proton-transfer step of the sequence of reactions catalyzed by triosephosphate isomerase (TIM) and focus on questions related to "promoting" modes. More detailed discussions of other issues, such as comparing tunneling in the enzyme to that in the gas phase and solution, are left to a separate publication.[52] The computational details are summarized in section II, and the results are presented in section III. The discussion and conclusions are given in section IV.

II. Computational Models

II.1. Model Proton-Transfer Reactions. To clarify the definition and effect of coupled vibrational modes (both "promoting" and "demoting" modes) and to relate the present analysis to other work, we first use simple model potential energy functions for the proton-transfer reaction. The proton-transfer coordinate, q, is modeled by a symmetric double-well potential given by a quartic polynomial (see Figure 1)

$$V^{1d}(q) = V_0(q^2 - 1)^2 \qquad (1)$$

where V_0 is the barrier height at $q = 0$; the two minima have zero-energy and are at $q = \pm 1$.

In the two-dimensional model, an additional "orthogonal" degree of freedom is considered. It is either symmetrically (Q, see Figure 2) or antisymmetrically (x, see Figure 3) coupled to the proton-transfer coordinate, q. As discussed in the Introduction,[23,25] the Q vibration may correspond to the donor−acceptor stretch (see Figure 2), whereas the x vibration typically corresponds to a bath mode that favors a localized charge distribution and therefore requires reorganization after the proton transfer (see Figure 3). In general, the proton-transfer coordinate does not have symmetry (e.g., the donor and acceptor atoms are different), so that the coupled modes are not symmetric or antisymmetric. However, for these model systems, symmetry is assumed for simplicity of analysis. The corresponding potential energy functions are

$$V^{2d-S}(q,Q) = V_0(q^2 - 1)^2 + \frac{1}{2}M\Omega^2\left(Q + \frac{Cq^2}{M\Omega^2}\right)^2 \quad (2a)$$

$$V^{2d-A}(q,x) = V_0(q^2 - 1)^2 + \frac{1}{2}m\omega^2\left(x - \frac{cq}{m\omega^2}\right)^2 \quad (2b)$$

where $C(c)$ is the coupling strength and $\Omega(\omega)$ is the vibrational frequency for the orthogonal mode. As in the 1D model (eq 1), the barrier heights in both cases are V_0, and the saddle point is still at (0,0); the minima are at $(\pm 1, -C/M\Omega^2)$ and $(\pm 1, \pm c/m\omega^2)$ for the symmetric and antisymmetric case, respectively. The barrier frequency is $i[4V_0/m]^{1/2}$ for both the 1D and symmetric-2D case, but it is $i[4V_0/m - c^2/m\omega^2]^{1/2}$ for the antisymmetric-2D case; that is, the presence of the antisymmetric coupling gives rise to a lower barrier frequency. With the parameters used for Figures 2 and 3 (see Table 1), the barrier frequencies are $838i$ cm^{-1} and $800i$ cm^{-1}, respectively. The parameters were chosen such that the barrier height and frequency are similar to those found in calculations for the hydride transfer in horse liver alcohol dehydrogenase;[34] they are close to the values in ref 25a.

In the third model (see Figure 4), two orthogonal degrees of freedom are considered; one is symmetrically coupled and the other antisymmetrically coupled to q. The functional form for the potential, which was suggested in ref 25a, is

$$V^{3d}(q,Q,x) = V_0(q^2 - 1)^2 + \frac{1}{2}M\Omega^2\left(Q + \frac{Cq^2}{M\Omega^2}\right)^2 + $$
$$\frac{1}{2}m\omega^2\left(x - \frac{cq}{m\omega^2} - \frac{dQ}{m\omega^2}\right)^2 \quad (3)$$

where d is the strength of the coupling between the symmetric and antisymmetric modes.

The motivation for studying the above models is that similar problems have been discussed by a number of authors in the context of vibrational effects on proton transfer (see the Introduction). One limitation is that, because of the specific form of the potential used here, the proton-transfer distance along q changes very little as Q is excited. For example, the equilibrium values of q are approximately $\pm(1 - C^2/2M\Omega^2V_0)$ and $\pm(1 - c^2/4m\omega^2V_0)$ for the symmetric and asymmetric case, respectively, when Q and x are zero, respectively; that is, the proton-transfer distance changes less than 0.05 bohr with the current set of parameters (Table 1) compared to a value of 2 bohr in the uncoupled 1D model. This is to be contrasted to more realistic situations where the transfer distance is decreased substantially when the donor−acceptor vibration is excited (e.g., in the case
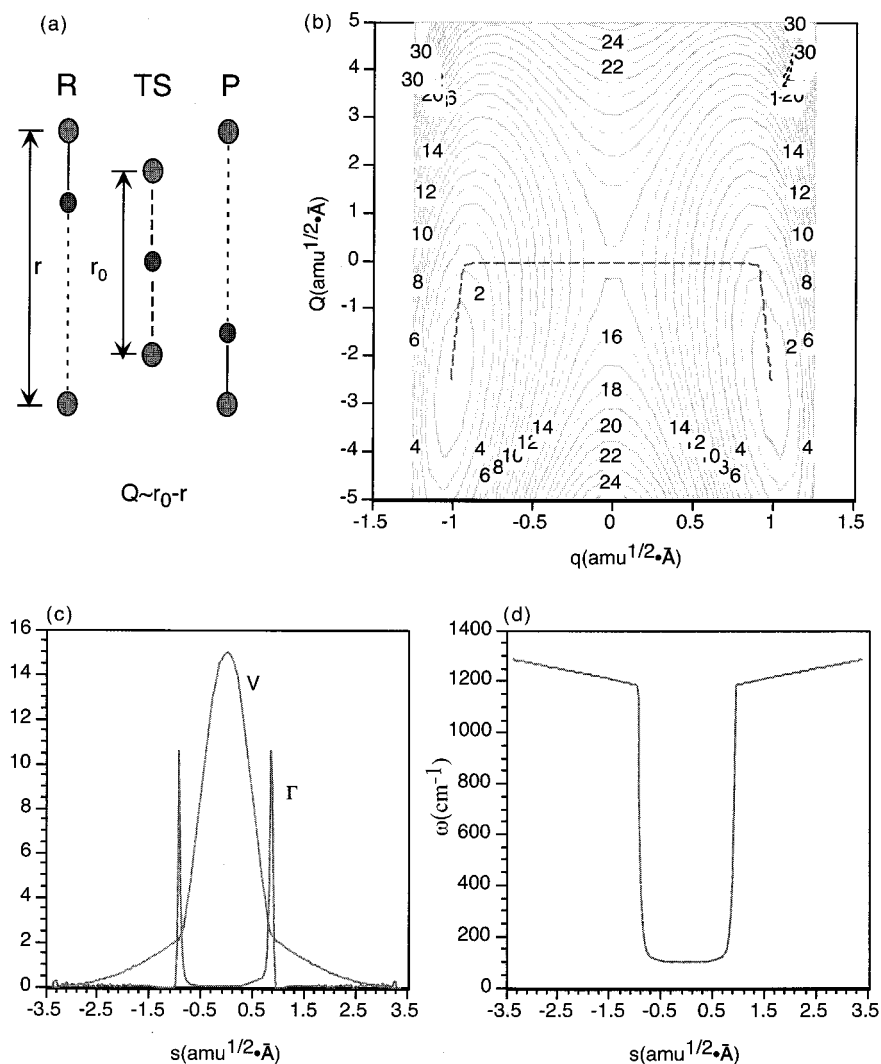
Figure 2. 2D model in which a mode is symmetrically coupled to the proton-transfer coordinate. (a) A schematic illustration of a typical symmetric mode, Q, which is related to the donor−acceptor stretch; note that no reorganization is required between the reactant (R) and product (P), but a substantial displacement occurs in the transition state (TS); (b) The potential energy surface and the minimum energy path (dot line); (c) Potential energy and the reaction path curvature along the minimum energy path; (d) Vibrational frequency orthogonal to the reaction coordinate along the reaction path. The energies are given in kcal/mol, the reaction path curvature is given is $amu^{-1/2}$ $bohr^{-1}$, and the frequencies are given in cm^{-1}.

of TIM, the proton-transfer distance changes by up to 0.4 Å when the donor−acceptor distance is varied; see section III.3). In some earlier studies,[23,24,25,26] a Marcus-type treatment for the proton transfer was invoked.[35] The reaction coordinate was taken to be the heavy atom vibration (Q,x), rather than the coordinate involving the proton. In this analogy to the Marcus model for electron transfer,[36] it is assumed that the minimum energy path (MEP) is irrelevant;[37] that is, the proton motion is fast compared to the heavy atom vibrations, and as in the electron-transfer case,[38] it is the "solvent coordinate" (e.g., the donor−acceptor distance) that determines whether reaction takes place; for example, a Franck−Condon factor related to the reorganization of the "solvent coordinate" has to be considered when the coupling is antisymmetric (see above). Thus, it might appear that there is conceptual conflict between the VTST approach, which is based on the potential energy surface *in the neighborhood of* the MEP and the Marcus type of treatment. We use the model systems to demonstrate that the two approaches give consistent descriptions for proton transfer reactions. Moreover, the results indicate that the MEP picture is satisfactory for proton transfer reactions at room temperature. For many systems, tunneling along paths with strong deviation from MEP ("deep

tunneling") is expected to occur only at low temperatures. In a separate publication, the issue of reaction coordinate for proton transfer at different temperatures will be treated more quantitatively with centroid path−integral techniques.[39]

To extend the model system results to a somewhat more realistic yet simple system, we treat the intramolecular proton transfer in an enediolate molecule (see Figure 8). This system was used in earlier studies[52,39] to represent one of the proton-transfer steps in triosephosphate isomerase. The enediolate molecule was treated with a modified AM1 parameter set (AM1-SRP) derived by fitting B3LYP/6-31+G(d,p) level results.[59] Test calculations showed that the specific AM1 set of parameters is very accurate for the intramolecular proton-transfer reaction we are studying here. The barrier heights without zero-point energy are 9.5 and 9.0 kcal/mol at the AM1-SRP and B3LYP/6-31+G-(d,p) levels, respectively, and the imaginary frequency at the saddle point is $1365i$ cm^{-1} at the AM1-SRP level and $1379i$ cm^{-1} at the B3LYP/6-31+G(d,p) level.

II.2. Proton Transfer in Triosephosphate Isomerase (TIM). As mentioned above in the Introduction, the simple models cannot capture all of the essential features of realistic proton transfer reactions. In particular, tunneling is highly sensitive to
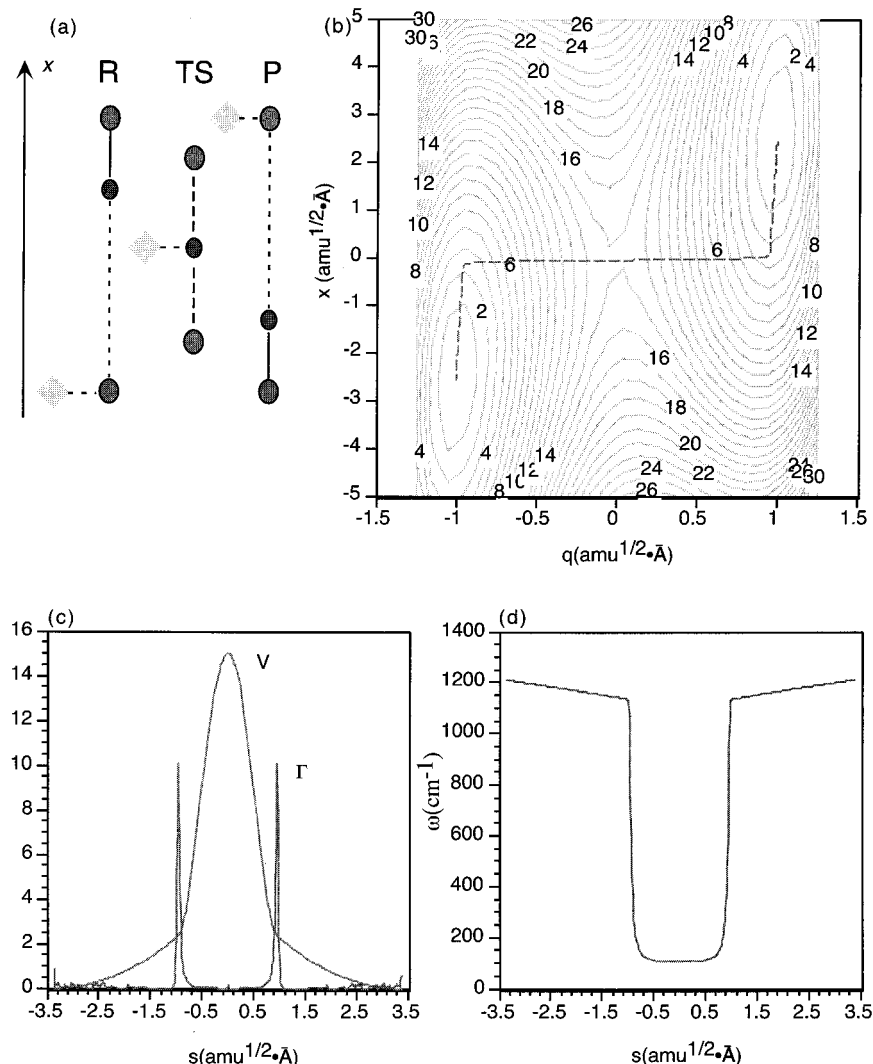
Enzyme-Catalyzed Proton Transfer Reactions

J. Phys. Chem. B, Vol. 106, No. 32, 2002 **7931**

Figure 3. 2D model in which a mode is antisymmetrically coupled to the proton-transfer coordinate. (a) A schematic illustration of a typical antisymmetric mode, x, which is related to a solvent degree of freedom, which favors negative charges and therefore a reorganization occurs going from the reactant (R) to the product (P); (b) The potential energy surface and the minimum energy path (dot line); (c) Potential energy and the reaction path curvature along the minimum energy path; (d) Vibrational frequency orthogonal to the reaction coordinate along the reaction path. The energies are given in kcal/mol, the reaction path curvature is given is amu$^{-1/2}$ bohr^{-1}, and the frequencies are given in cm^{-1}.

TABLE 1: Parameters and Properties of Model Potential Functions Used in the Current Work^a

| parameter/property | 1D | 2D | | 3D | | | |
		symmetric	antisymmetric	case I	case II	case III	case IV
V_0 (kcal/mol)	15.0	15.0	15.0	15.0	15.0	15.0	15.0
m_q (amu)	1.0079	1.0079	1.0079	1.0079	1.0079	1.0079	1.0079
Ω (cm^{-1})		100.0		100.0	100.0	100.0	100.0
ω (cm^{-1})			100.0	25.0	25.0	25.0	25.0
M (amu)		100.0		100.0	100.0	100.0	100.0
m (amu)			100.0	250.0	250.0	250.0	250.0
C (a.u.)		5×10^{-3}		5×10^{-3}	5×10^{-3}	5×10^{-3}	5×10^{-3}
c (cm^{-2})			2.5×10^5	0.0	2.5×10^4	0.0	2.5×10^4
d (kcal/mol·Å^{-2})				0.0	0.0	15.0	15.0
$V^{\neq}/V_a^{\neq}$ (kcal/mol)	15.0/13.3	15.0/13.2	15.0/13.3	15.0/13.2	15.0/13.2	15.0/13.2	15.0/13.2
$\omega^{\neq}$ (cm^{-1})	838i	838i	800i	838i	836i	838i	836i

^{a} For the definition of parameters, see eqs 1−3 in the text; $V^{\neq}$ and $V_a^{\neq}$ are the barrier height without and with the zero-point energy correction, respectively; $\omega^{\neq}$ is the barrier frequency.

the shape and height of the proton transfer barrier, which changes in a highly anharmonic manner as the donor−acceptor distance varies. A system for which such effects are included is provided by the first proton-transfer step in TIM. TIM catalyzes the interconversion of dihydroxyacetone phosphate (DHAP) and *R*-glyceraldehyde-3-phosphate (GAP), an important

step in the glycolytic pathway. Recently, we have carried out detailed studies of the catalytic mechanisms[59] of TIM and the importance of tunneling in determining the proton-transfer rate constants and isotope effects by use of the VTST approach.[52] In this paper, we focus on questions related to the "promoting" modes in TIM and focus on the first step in the overall reaction,
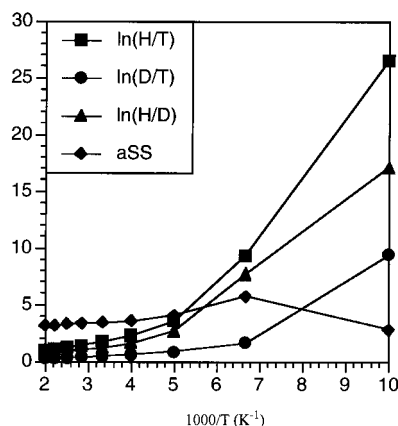
Figure 4. Logarithm of kinetic isotope effects and the SSE as a function of temperature for the 1D model (see eq 1 and Table 1 for the parameters used); a similar behavior is found for the 2D models.

which corresponds to the proton transfer from the DHAP substrate C_α to the oxygen atom in the side chain of Glu165 (see Figure 11). As described in detail elsewhere,[59] we employed stochastic boundary conditions[40] for the enzyme−substrate system, and the potential energy was represented by a combined QM/MM approach[41] in which the substrate and Glu165 were treated with AM1-SRP[42,59] and the rest of the system was treated with the CHARMM22 force field. To reduce the cost of the rate constant calculations (see section II.3), atoms that are relatively far from the active site were fixed in the reaction path and normal mode calculations. In the "small" model, all atoms beyond 4 Å of the C_γ in the substrate (see Figure 1) were fixed; this results in a system consisting of 106 movable atoms, including 6 residues (Lys 12, His 95, Glu 165, Ile 170, Gly 210, Gly 231) and one water molecule. In the "larger" model, atoms beyond 8 Å of the C_γ were kept fixed; this results in 445 movable atoms, including 16 water molecules. The fixed environment, which complete the sphere, consists of 2235 atoms in the small model and 1895 atoms in the larger model. To determine the effect of the donor−acceptor stretch, the "promoting mode", a number of calculations with fixed donor−acceptor distances were carried out with the small model.

In the analysis of normal modes, participation ratios [43,44] were computed. Two quantities, R_i^{I} and R_i^{II}, are defined for each normal mode, k; they are

$$R_k^{\mathrm{I}} = \sum_j^{3N} L_{jk}^4 \tag{4a}$$

$$R_k^{\mathrm{II}} = \sum_i^{M_{\mathrm{res}}} [\sum_j^{3N_i} L_{jk}^2]^2 \tag{4b}$$

where L_{jk} is the jth element of the kth eigenvector, N and N_i are the number of atoms in the whole system and in the ith residue, respectively, and M_{res} is the number of residues in the system. The inverse of R_k^{I} indicates the number of atoms involved in the kth normal mode, and the inverse of R_k^{II} corresponds approximately to the number of residues involved.

II.3. Rate Constant Calculations. Rate constant calculations including tunneling were carried out for the proton-transfer reactions using the semiclassical variational transition-state theory (VTST). As discussed in detail elsewhere,[32] the VTST approach is formulated based on the properties of the potential energy surface in the neighborhood of the minimum energy path (MEP). In VTST, the effect of barrier recrossing is reduced by

letting the transition state deviate from the saddle point *along* the reaction coordinate and optimizing its position by variationally minimizing the reaction flux. This corresponds to searching for the free energy maximum along the reaction coordinate in the canonical ensemble (CVT). The effect of tunneling is taken into account by computing the one-dimensional WKB integral along a given path. In the small-curvature tunneling (SCT) limit, the tunneling path is taken to be the MEP, and the multidimensional corner-cutting effect[45] is taken into account by modifying the mass of the tunneling particle based on the reaction path curvature.[46] In the large-curvature limit (LCT),[47] the tunneling path is assumed to be the straight-line path connecting the points on the two sides of the barrier (i.e., with little movement of the heavy donor/acceptor atoms). Benchmark calculations on systems in which either accurate quantum mechanical results[48] or precise experimental rate constants[49] are available have demonstrated that the VTST approach is sufficiently accurate for medium size systems to be useful for the questions that are being considered here; that is, the methods (especially the LCT approach) are expected to give reliable results for the temperature dependence of rate constants, which is essential for the discussion of vibrational effects on proton transfers.

For the model systems with analytical potentials, rate constant calculations were carried out at both the SCT and LCT levels. For the enediolate molecule and enzyme, only small curvature tunneling (SCT) calculations were performed because LCT calculations are too computationally demanding, particularly for the enzyme system; the SCT calculations are sufficient for the qualitative behaviors that we are considering here, as indicated by path-integral simulations (Cui, Karplus, unpublished). In the SCT calculations for the enzyme, saving the eigenvectors at many points is very memory intensive. We have therefore implemented an algorithm to evaluate the reaction path curvature components in the TRAVEL module of CHARMM.[50] This allows us to use the conjugate peak refinement (CPR) algorithm[51] to optimize the MEP for large systems and reduces the memory requirement of the computation dramatically. Only the frequencies and the curvature components along the MEP have to be saved in disk or memory; they form two arrays that are linear in the size of the system. The required information (geometries, energies, frequencies, and curvature components along the MEP) is then used as input for a previously modified[52] version of POLYRATE 8.0[53] to calculate the effective reduced mass along the MEP, the tunneling integrals, and the rate constants. Between 70 and 110 points along the reaction coordinate were used in the VTST-SCT calculations. Of these, at least 50 points were in the critical region with the mass-weighted reaction coordinate in the range of $(-3.0, +3.0)$ amu$^{1/2}$ bohr. Test calculations with 320 points gave transmission coefficients within a factor of 1.2 at 300 K, indicating that the results with 50 points are sufficiently accurate for the present analysis.

The reaction parameters that are calculated are the rate constant k and the tunneling contribution, κ, where κ is defined as

$$\kappa(T) = \kappa^{\mathrm{CVT}} \frac{\int P_{\mathrm{1d}}^{\mathrm{G}}(E) \mathrm{e}^{-E/k_B T}\, \mathrm{d}E}{\int h\{E - V_{\mathrm{A}}^{\mathrm{G}}[s_*^{\mathrm{CVT}}(T)]\} \mathrm{e}^{-E/k_B T}\, \mathrm{d}E} \tag{5}$$

Here $h(E)$ is the Heaviside function, κ^{CVT} is the correction factor relative to TST due to the change in the position of the transition state (s_*^{CVT}) in canonical VTST, and the other factor corresponds to the tunneling correction to CVT, in which $P_{\mathrm{1d}}^{\mathrm{G}}(E)$ is the calculated 1D transmission (tunneling) coefficient at energy E.

Enzyme-Catalyzed Proton Transfer Reactions

J. Phys. Chem. B, Vol. 106, No. 32, 2002 **7933**

TABLE 2: Tunneling Coefficients, Representative Tunneling Energies, Rate Constants, and Kinetic Isotope Effects for 1D and 2D Model Proton Transfer Reactions at Different Temperatures[a]

| T(K) | property | 1D | | | | | | | symmetric | antisymmetric |
		uncoupled	$Q = -2.5$	$Q = -1.5$	$Q = 0.0$	$x = -2.5$	$x = -1.5$	$x = 0$	2D	2D
300	κ	2.2	2.6	2.4	2.1	1.9	2.0	2.0	2.2 (2.2)	2.0 (2.0)
	$\log k$	3.4	1.7	3.2	5.5	1.3	3.0	5.4	3.5 (3.5)	3.4 (3.4)
	E_{tul}	14.96	17.35	15.28	12.18	17.91	15.61	12.33	14.94 (14.96)	15.13 (15.13)
	k_H/k_D	3.5	4.2	4.0	3.9	3.4	3.4	3.4	3.8 (3.8)	3.4 (3.4)
	α_{SS}	3.46	3.53	3.51	3.46	3.47	3.41	3.43	3.47 (3.53)	3.44 (3.43)
200	κ	10.8	27.8	17.6	10.2	6.2	7.0	7.4	12.3 (12.5)	7.9 (7.4)
	$\log k$	−0.9	−3.2	−1.1	2.2	−4.3	−1.7	1.9	−0.7 (−0.7)	−1.0 (−1.0)
	E_{tul}	14.09	14.27	13.84	11.33	17.31	14.98	11.68	13.93 (14.11)	14.45 (14.48)
	k_H/k_D	15.4	35.7	25.2	17.0	10.7	11.3	11.9	18.7 (19.9)	12.4 (11.9)
	α_{SS}	4.07	4.47	4.24	3.96	3.87	3.80	3.87	4.06 (4.20)	3.92 (3.88)
100	κ	2.1×10^{12}	1.1×10^{16}	3.3×10^{13}	9.5×10^{9}	2.6×10^{5}	1.3×10^{7}	2.8×10^{9}	1.5×10^{11} (1.1×10^{13})	1.8×10^{10} (1.3×10^{10})
	$\log k$	−4.4	−6.2	−4.0	−0.5	−17.6	−10.9	−1.4	−5.3 (−3.5)	−6.4 (−6.4)
	E_{tul}	1.87	1.88	1.90	1.94	12.48	8.24	1.88	3.84 (2.36)	4.06 (4.01)
	k_H/k_D	2.8×10^{7}	2.4×10^{8}	3.2×10^{7}	1.2×10^{6}	8.6×10^{3}	3.4×10^{4}	1.6×10^{6}	3.1×10^{6} (1.5×10^{8})	3.7×10^{6} (8.7×10^{6})
	α_{SS}	2.82	2.57	2.63	2.74	3.21	2.67	3.00	2.68 (2.88)	2.91 (3.18)

[a] The κ is the tunneling coefficient, k is the rate constant in s^{-1}, E_{tul} (in kcal/mol) is the representative tunneling energy which is defined as the energy at which the product of the transmission coefficient and the Boltzmann factor at a given temperature is maximal; k_H/k_D is the H/D kinetic isotope effect, and α_{SS} is the Swain-Schaad exponent defined as $\ln(k_H/k_T)/\ln(k_D/k_T)$. The numbers without parentheses were obtained at the SCT level, and these with parentheses were obtained at the LCT level. The zero of energy is the reactant *without* the zero-point energy.

To avoid confusion, we note that κ is often referred to as the tunneling coefficient; here we use the term "tunneling contribution" to emphasize the fact that it is a correction to the classical rate constant and distinguish it from the transmission (tunneling) coefficient, $P_{1d}^{G}(E)$, which is an energy-dependent factor (see discussion in relation to the work of Hynes et al.[23] in section III.1). The representative tunneling energy, E_{tul}, is also determined. It is defined as the energy at which the product of the Boltzmann factor and tunneling(transmission) coefficient, $P^{WKB}(E)$, is maximal.[54] This quantity is used to characterize the major contribution to tunneling at a given temperature. For example, a high E_{tul} suggests that tunneling occurs mainly at the energy slightly below the barrier, and the tunneling path is expected to be close to the minimum energy path; by contrast, a low E_{tul} suggests that tunneling occurs mainly at energy close to the ground vibrational level, and therefore, corner-cutting paths are expected to be more important (a more quantitative discussion related to this using centroid path-integral techniques will be published elsewhere). We also briefly discuss the temperature dependence of the kinetic isotope effect and the Swain—Schaad exponent (SSE); the latter is defined as $\ln(k_H/k_T)/\ln(k_D/k_T)$.[55] The SSE, particularly for the hydrogen at the secondary position, has been used in experimental analyses to indicate that tunneling is significant to enzyme-catalyzed proton-transfer reactions.[12,14−17] Although our calculations for TIM catalyzed reactions suggest that the correlation between the magnitude of the SSE and the contribution of tunneling is not very strong,[34] we examine whether the behavior of these quantities reflect the effect of promoting vibrational motions.

III. Results and Discussions

In this section, we present first the results for the low-dimensional models to clarify the meaning and the effect of promoting and demoting modes. The results are discussed in the VTST framework and compared to the treatments based on a Marcus-type description. We then analyze the symmetric and antisymmetric mode contribution in a real molecule, the enediolate in the gas phase. Finally, we treat the first proton transfer in TIM and identify the important vibrational modes. On the basis of these results, we discuss both the identity and the nature of the modes in enzymes in section IV.

III.1. Model Proton-Transfer Reactions. *One-Dimensional System.* In one dimension, the semiclassical VTST based on the WKB approximation is expected to be highly accurate. As shown in Table 2, the tunneling contribution, κ, is only of 2.2 at 300 K, which is consistent with the relatively low barrier frequency, 838i cm^{-1}. However, at low temperatures, tunneling becomes very large; at 100 K, κ equals $10^{12.3}$. The representative tunneling energy (E_{tul} in Table 2) is very sensitive to the temperature; it is close to the barrier top for temperatures above 200 K and is very close to the bottom of the potential well, 1.87 kcal/mol above the bottom of the well (i.e., only 0.002 kcal/mol above the zero point level) at 100 K. This is consistent with the fact that the reaction proceeds entirely via tunneling at the lower temperature. The H/D kinetic isotope effect has a monotonic behavior, as expected, and increases exponentially as the temperature is lowered; it is 3.5, 15.4, and 2.8×10^7 at 300, 200, and 100 K, respectively. The SSE shows a nonmonotonic behavior as a function of the temperature (see Table 2

and Figure 4); it first increases as the temperature is lowered from 300 to 150 K and then decreases as the temperature is lowered further. Numerically, this arises because the value of $\ln(k_D/k_T)$ increases rapidly at temperatures below 150 K, so that the ratio $\ln(k_H/k_T)/\ln(k_D/k_T)$ becomes smaller. Physically, this corresponds to the fact that D starts to tunnel significantly below 150 K; with the parameters (barrier frequency) shown in Table 1, the semiclassical estimate, given by $\hbar\omega^{\ddagger}/2\pi k_B$,[56] for the crossover temperatures (i.e., the temperature at which the proton transfer changes character from a thermally activated process to one that is tunneling dominated) are 190, 135, and 110 K for H, D, and T, respectively.

Transfer with a Symmetrically Coupled Mode (eq 2a, Figure 2a). In the presence of the symmetrically coupled mode, Q, the TST rate constant is very similar to the 1D case because the two models have the same barrier height and differ only slightly in the reactant vibrational frequencies (1185 and 1286 cm^{-1}, respectively). The rate constants including tunneling, however, are very different, and the result depends substantially on the level of theory used for treating tunneling. At temperatures above 200 K, the SCT and LCT rate constants are very similar, and both are larger than the 1D WKB rate constant (see Table 2, note that SCT/LCT is not defined for 1D). The tunneling contributions, κ, obtained at 300 K and at 200 K with the three methods are similar; that is, they are 12.5, 12.3, and 10.8 at 200 K for LCT-2D, SCT-2D, and WKB-1D, respectively. At both the SCT and LCT levels, the tunneling contribution is always significantly more at lower temperature. At lower temperature, however, only the LCT results are satisfactory and larger than the 1D rate constants, and the SCT underestimates the effect of tunneling (and therefore the rate constant) substantially; at 100 K, the tunneling contributions are $10^{13.0}$, $10^{11.2}$, and $10^{12.3}$ for LCT-2D, SCT-2D, and WKB-1D, respectively. Consistent with the larger tunneling contribution, the symmetric 2D case gives large H/D isotope effects compared to the 1D model at all temperatures (Table 2); the SCT calculation underestimates the value at low temperatures where the calculated tunneling is too small. At all levels, the H/D isotope effect varies monotonically as a function of temperature, as expected. The SSE follows the same nonmonotonic trend as in the 1D model, and the values are also very similar at all temperatures. These observations have implications for recent experiment on the thermophilic alcohol dehydrogenase (see section IV.).

To examine the origin of effect resulting from the symmetric mode, Q, we plot one-dimensional cuts along the q coordinate at different Q values and compare these with the uncoupled 1D potential (see Figure 1a). We also compute the effective rate constant and tunneling contribution with a 1D calculation along the proton-transfer coordinate at fixed Q value and temperature T. These results are referred to as $k^{1d}(T;Q)$ and $\kappa^{1d}(T;Q)$, respectively; they are also listed in Table 2. As is widely recognized,[10,23] the 1D "effective q potential" has a smaller barrier at vibrationally excited Q compared to that at the equilibrium Q value; for example, the effective barrier at $Q = 0$ is 12.7 kcal/mol, and it is 17.4 kcal/mol at $Q = -2.5$ amu$^{1/2}$ Å (the equilibrium Q value), which are 2.3 kcal/mol lower and 2.4 kcal/mol higher, respectively, than the adiabatic barrier height of 15.0 kcal/mol (in both uncoupled 1D and 2D). It has been less emphasized in the literature, however, that the effective barrier frequency also changes substantially as Q varies; it is 838i and 908i cm^{-1} at $Q = 0$ and -2.5 amu$^{1/2}$ Å, respectively. Therefore, one would expect that tunneling plays a more significant role at Q near equilibrium (e.g., $Q = -2.5$ amu$^{1/2}$
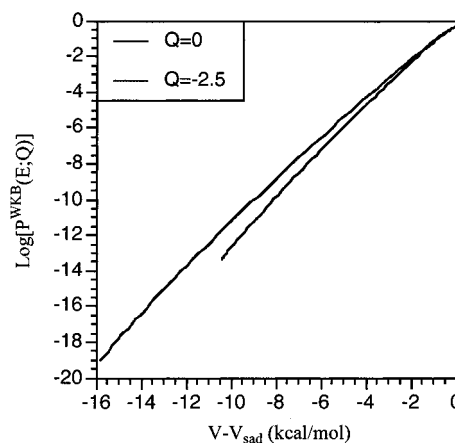

Figure 5. Tunneling (transmission) coefficient (in log) as a function of the energy measured from the top of the barrier for the effective potential along the proton transfer coordinate with the symmetrically coupled mode fixed at the equilibrium ($Q = -2.5$ amu$^{1/2}$ bohr) and excited value at the saddle point on the 2D potential energy surface (0.0 amu$^{1/2}$ bohr). The curve is "shorter" for $Q = 0.0$ because the effective barrier is lower (see text).

Å), where the barrier is both high and narrow, as compared to the large Q displacement (e.g., $Q = 0$). This is confirmed by the results shown in Table 2. At 200 K, for example, the tunneling contributions for the 1D effective potentials at $Q = -2.5$, -1.5, and 0.0 amu$^{1/2}$ Å are 27.8, 17.6, and 10.2, respectively; the value for the uncoupled 1D case is 10.8, very similar to the value at $Q = 0.0$ amu$^{1/2}$ Å. At 100 K, the Q dependence of the tunneling contribution is much more pronounced, and the corresponding values are $10^{16.0}$, $10^{13.5}$, $10^{10.0}$, and $10^{12.3}$, respectively. The H/D isotope effect follows the same trend as the tunneling contribution; i.e., the values are larger at Q near the equilibrium value (e.g., the isotope effect is 35.7, 25.2, and 17.0 for $Q = -2.5$, -1.5, and 0.0, respectively, at 200 K). At temperatures above 200 K, the SSE is larger when the tunneling contribution is larger; for example, it is 4.47, 4.24, and 3.96 for $Q = -2.5$, -1.5, and 0.0, respectively, at 200 K. At low temperature where D also tunnels significantly, the trend is reversed because the value of $\ln(k_D/k_T)$ becomes very important; the values are 2.57, 2.63, and 2.74 at 100 K for $Q = -2.5$, -1.5, and 0.0, respectively.

It is interesting to compare the present results that the *contribution of tunneling* to the rate constant, which is characterized by $\kappa^{1d}(T;Q)$ in the current work, decreases as Q is vibrationally excited with the view that the Q vibration "promotes" tunneling, as stated by Borgis et al.[23] There are two major differences between the two descriptions. First, Borgis et al.[23] were referring to the magnitude of the tunneling matrix element, which can be related to the tunneling (transmission) coefficient at low energy, whereas $\kappa^{1d}(T;Q)$ reflects the contribution of tunneling to the thermal rate constant and therefore also depends on the classical barrier height. In Figure 5, we compare the 1D tunneling (transmission) coefficient, $P^{WKB}(E;Q)$ (to be distinguished from the tunneling contribution, κ), at different energies for $Q = -2.5$ and 0.0 amu$^{1/2}$ Å. At low energies in the proton-transfer coordinate, the tunneling coefficient is indeed larger when the Q vibration is excited; this is in agreement with the previous discussion.[23] However, the effective barrier also decreases quickly with vibrational excitations, so that the classical rate constant increases exponentially as Q becomes vibrationally excited. As a result, the *contribution of tunneling* to the effective thermal rate constant, $\kappa^{1d}(T;Q)$, drops as Q is vibrationally excited if the change in the classical

Enzyme-Catalyzed Proton Transfer Reactions

J. Phys. Chem. B, Vol. 106, No. 32, 2002 **7935**

rate constant is more significant than the change in the tunneling coefficient. This is the case for the present model. Borgis et al.[23] used a perturbative treatment to obtain the proton-transfer rate constant which assumes that tunneling occurs only through the ground vibrational state along the proton transfer coordinate. This assumption is valid only at low temperatures. As indicated by E_{tul}, the proton transfer at room temperature is dominated by tunneling just under the top of the barrier (see Table 2). At this energy, as shown in Figure 5, the tunneling (transmission) coefficient is smaller when Q is vibrationally excited. This results from the fact that the effective barrier frequency (i.e., the barrier frequency for the effective potential along the proton-transfer coordinate at fixed Q value) is lower when the Q vibration is excited. For a more detailed analysis, see the Supporting Information.

Having demonstrated the effect of the promoting modes, a relevant question is how to identify such modes in realistic systems. Using a similar 2D-symmetric model potential coupled to a harmonic bath, Schwartz and co-workers[25] suggested that one should observe the contribution of the Q mode(s) when plotting the spectral density along the q coordinate. Here we look at the problem in the VTST framework. At high temperature, as discussed above, the minimum energy path picture is qualitatively correct. The character of the reaction coordinate is very different around the reactant (product) and the saddle point along the minimum energy path; that is, it is mainly the Q vibration around the reactant (product) and is proton transfer (q motion) around the saddle point. In other words, the reaction path is highly curved, and the reaction path curvature (Γ) is large in the region where the character of the reaction coordinate changes rapidly (see Figure 2b). The vibrational frequency of the mode orthogonal to the reaction path also changes abruptly in the same region because of the significant mixing of the (q,Q) degrees of freedom; because the nature of the reaction coordinate switches quickly from Q to q, the mode orthogonal to the reaction coordinate in this simple system changes its nature quickly as well. The vibrational frequency in the orthogonal mode (765 cm^{-1}) at the configuration where Γ is peaked is much higher than the "intrinsic" frequency of the promoting mode Q (100 cm^{-1}). In principle, to obtain the "intrinsic" frequency of the promoting mode, one would monitor the rapidly varying frequency (which also gives the large reaction path curvature component) until it decouples from the barrier mode in the transition-state (TS) region (see Figure 2d). This is expected to be very difficult for macromolecules in which the vibrational spectrum is denser. Instead, one may find the intrinsic frequencies based on the overlap with the modes at the TS or reactants. In the current work, we perform the projection based on the TS because the curvature peak usually occurs close to the saddle point (see sections III.2 and III.3).

Transfer with an Antisymmetrically Coupled Mode (eq 2b, Figure 3a). Table 2 shows that both the tunneling contribution and rate constant for the antisymmetric 2D case are smaller than these in the symmetric 2D and uncoupled 1D case. Therefore, the VTST result agrees with the general consideration that antisymmetric coupling decreases tunneling and the rate of transfer;[21,25,28] that is, it has a "demoting effect" if the uncoupled proton transfer is taken as the reference. For a more detailed analysis, see the Supporting Information. Consistent with the behavior of the tunneling contribution, the antisymmetric 2D case gives lower H/D kinetic isotope effects compared to the symmetric 2D and the uncoupled 1D models (see Table 2). For the 1D cuts, the trend in H/D KIE follows that of the tunneling contribution; that is, the value increases as the x vibration is

excited. Compared to the 2D-symmetric cases, the SSE is less correlated with the magnitude of the tunneling contribution. For example, the tunneling contributions are 6.2, 7.0, and 7.4 at 200 K for $x = -2.5$, -1.5, and 0.0, respectively; the corresponding SSE are 3.87, 3.80, and 3.87, respectively. The point that SSE cannot be clearly correlated with the magnitude of tunneling has been emphasized in our earlier work on TIM.[52]

Because the reaction path is highly curved in both the symmetric and antisymmetric 2D models, the profiles for the reaction path curvature and the orthogonal vibrational frequency are very similar in the two cases (see Figure 2d and 3d). Therefore, it is difficult to distinguish a symmetrically and an antisymmetrically coupled mode based solely on the reaction path curvature. However, once modes with large reaction path curvatures are known, it is straightforward to determine their characters (i.e., symmetric or antisymmetric) based on the associated displacement vectors in the reactant and product relative to the saddle point (see section III.2).

Transfer with More than One Coupled Mode. Finally, we briefly examine a model system in which both a symmetric and an antisymmetric mode are present. The model is used to examine the relation between the coupling among different modes, reaction path properties and the magnitude of tunneling.

Four different sets of parameters were used in eq 3 to represent different couplings (see Table 1); when both c and d are set to zero, it reduces to the symmetric 2D model (case I); when d is zero, the proton transfer is coupled to both symmetric and antisymmetric modes, but there is no explicit coupling between the latter two (case II); when c is zero, the antisymmetric mode is coupled to the symmetric mode but not to the proton-transfer coordinate (case III). The most "realistic" scenario is case IV, in which the symmetric mode (Q) and the antisymmetric mode (x) are also coupled. We note that the specific form of the potential in eq 3 also gives an antisymmetric coupling term between Q and the proton-transfer coordinate. As shown in Figure 6, part a is identical to Figure 2c, though the scale is different. The three cases have two sets of peaks in the reaction path curvature; one major set is close to the saddle point (in the similar position as in part a), and the other smaller one is closer to the reactant/product. We note that mass-weighted coordinate was used for the reaction path length, s. The coupling between the antisymmetric and symmetric modes destroys the symmetry of the reaction and makes the second curvature peak in the product region more pronounced (see below). The profiles for the path curvature are very similar to that found in a model for a proton-transfer reaction in TIM (see section III.3). It is interesting, therefore, to demonstrate the origin of the second set of peaks.

As shown in Figure 7b, the initial stage of the reaction involves the rapid change of x until $s \sim -3$ amu$^{1/2}$ Å. There the character of the reaction coordinate becomes essentially the Q vibration, which in turn changes to the proton-transfer coordinate (q) starting from $s \sim -1$ amu$^{1/2}$ Å. Similar changes in the character of the reaction coordinate occur in the reverse order after the saddle point. Parallel to the variation in the character of the reaction coordinate, the frequencies orthogonal to the reaction coordinate undergo rapid changes in the corresponding regions (Figure 7c). Because of the coupling between x and Q, the reaction is asymmetrical (Figure 7a,b), and the saddle point is much closer to the product ($s \sim 5$ amu$^{1/2}$ Å) than to the reactant ($s \sim -9$ amu$^{1/2}$ Å). Thus, it clear that the outer set of peaks in the reaction path curvature (Figure 7a) is due to the change in the character of the reaction coordinate in the corresponding region, from the low frequency x motion
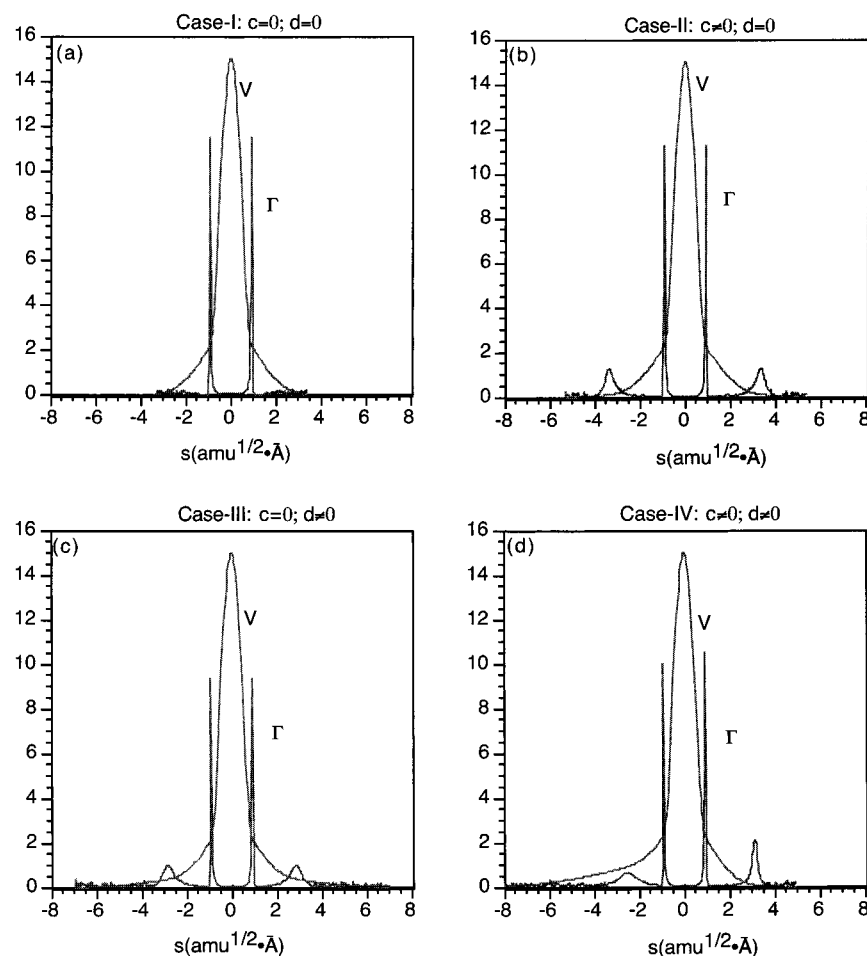
Figure 6. Energy and reaction path curvature along the minimum energy path for the four 3D models with different coupling coefficients. See eq 3 and Table 1 for the form of the potential and values for the coupling parameters.

(25 cm^{-1}) to the higher frequency Q motion (100 cm^{-1}). The peak in the product region is slightly higher because the change in the character of the reaction coordinate takes place more rapidly due to the form of the potential coupling between x and Q (see Figure 7b).

The SCT results (see Table 3) change very little among the four sets of models, which differ in the outer set of curvature peaks. This indicates that the outer set of curvature peaks have little to do with tunneling, in accord with the fact that the proton-transfer coordinate, q, hardly changes in that region (Figure 7b). The LCT results are very close to the SCT rates at temperatures above 200 K and are larger in magnitude at lower temperatures. Comparison of the four cases (see Table 3) shows that the coupling between the antisymmetric mode and the proton-transfer coordinate (nonzero c) decreases the LCT tunneling contribution substantially. The tunneling contribution is close to 10^{13} at 100 K for cases for c equals zero (cases I and III) and is smaller by up to an order of magnitude for cases with nonzero antisymmetric coupling (cases II and IV). The decrease is much more significant for case IV, in which the "symmetric" mode Q also has an antisymmetric coupling term with the proton coupling coordinate through the last term in eq 3. As a result, the symmetry in the (Q,q) potential surface is destroyed (compare Figure 7 parts d and e for the 2D cut with $x = 0$, and Figure 7f for 1D cut along q). This leads to the decrease of tunneling (see the discussion for the 2D antisymmetric model above). For example, the tunneling contribution across a 1D effective barrier along q (Figure 7f) with (Q,x) fixed at the values

$(-2.5$ amu$^{1/2}$ Å, 0.0) is $10^{15.6}$ at 100 K for case IV and $10^{15.8}$ for case III; for comparison, it is $10^{16.0}$ for case I.

III.2. Proton Transfer in the Model Enediolate. In the last subsection, we demonstrated the effects of symmetric and antisymmetric modes on proton transfer, and showed that the contribution of their couplings to the proton transfer coordinate are reflected in the reaction path curvature. Here, we use a small molecule to illustrate the symmetric and antisymmetric modes in a realistic system and expand our analysis of the connection between the coupling of modes to proton transfer and the reaction path curvature. This system can be regarded as a model for the intramolecular proton transfer, which has been proposed to take place in TIM but has been shown to be unlikely except in a mutant form.[52]

As shown in Figure 8a, the proton transfer in the model enediolate is a symmetric reaction, so that at the saddle point, modes can be separated into symmetric and antisymmetric types. The barrier for the reaction is 9.5 kcal/mol without zero-point energy and 7.0 kcal/mol with zero-point correction. The essential geometrical parameters (i.e., the donor/acceptor-proton distances and the donor−acceptor distance) vary along the reaction path in a manner similar to that in the model systems discussed in the previous section. Figure 8, parts b and d, shows that the initial stage of the reaction ($-2.5 < s < -0.5$ amu$^{1/2}$ bohr) involves mainly the decrease of the O−C−C bending angle and therefore the donor−acceptor (O^D−O^A) and acceptor−proton (O^A−H) distances, whereas the donor−proton (O^D−H) distance increases only slightly (to 1.067 Å from the equilibrium value 0.965 Å). Starting from s equal to about -0.5 amu$^{1/2}$ bohr, the

Enzyme-Catalyzed Proton Transfer Reactions

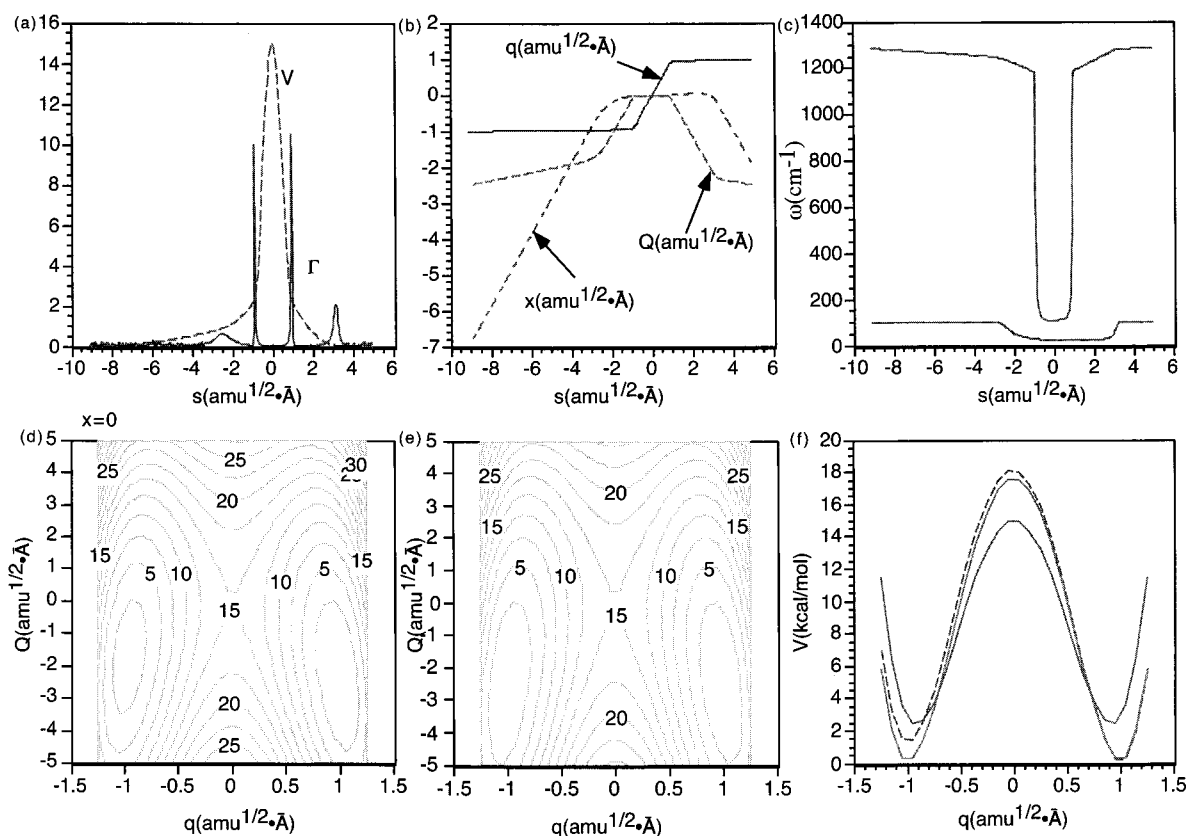*J. Phys. Chem. B, Vol. 106, No. 32, 2002* **7937**

Figure 7. (a) Energy and reaction path curvature along the minimum energy path for the case-IV 3D model. (b) Geometrical parameters along the minimum energy path; (c) Frequencies orthogonal to the reaction path; (d and e) 2D (Q, q) cuts of the potential energy surface with $x = 0$ for cases II and IV, respectively; note that the symmetry of the potential is destroyed in case IV due the coupling between Q and x vibrations; (f) 1D cuts (along q) of the potential energy surface with $x = 0$ and $Q = -2.5$ amu$^{1/2}$ Å; the lower solid line is for case I, the higher solid line is for case II, and the dashed line is for case IV. Once again, note the asymmetry caused by the $Q-x$ coupling (case IV).

TABLE 3: Tunneling Coefficients and Rate Constants for the 3D Models with Different Coupling Strength[a]

		case I $c = 0; d = 0$	case II $c \neq 0; d = 0$	case III $c = 0; d \neq 0$	case IV $c \neq 0; d \neq 0$
300 K	κ	2.2 (2.2)	2.2 (2.1)	2.2 (2.2)	2.2 (2.1)
	$\log k(\text{s}^{-1})$	3.52 (3.52)	3.52 (3.50)	3.52 (3.50)	3.52 (3.50)
200 K	κ	12.4 (10.4)	12.0 (10.1)	12.2 (10.8)	11.9 (10.0)
	$\log k(\text{s}^{-1})$	−0.71 (−0.70)	−0.72 (−0.80)	−0.71 (−0.76)	−0.72 (−0.80)
100 K	κ	1.5×10^{11} (1.1×10^{13})	1.0×10^{11} (6.0×10^{12})	1.5×10^{11} (9.7×10^{12})	1.0×10^{11} (1.0×10^{12})
	$\log k(\text{s}^{-1})$	−5.32 (−3.45)	−5.47 (−3.70)	−5.30 (−3.50)	−5.47 (−4.47)

^{a} The numbers without parentheses were obtained at the SCT level, and these with parentheses were obtained at the LCT level.

O^D−H distance increases rapidly to about 1.25 Å at the saddle point. The magnitude of the reaction path curvature (Γ) reaches a maximum of 2.3 amu$^{-1/2}$ bohr^{-1} at s equals to −0.5, as shown in Figure 8c. The effect of reaction path curvature on tunneling is significant even at room temperature. The SCT tunneling contribution is 7.7 at 300 K and only 3.3 if the curvature effect is not included (i.e., in a ZCT calculation). The difference is even larger at lower temperatures; it is about 10^4 at 100 K.

To examine which modes are significantly involved in the reaction, we plot the curvature components, $B_{m,\text{F}}$, of different vibrational modes at $s = -0.5$ in Figure 9a; the reaction path curvature component is given by[46]

$$B_{k,\text{F}}(s) = \mathbf{L}_k^{\text{T}} \frac{d\vec{\nu}}{ds} = -|g|^{-1} \mathbf{L}_k^{\text{T}} \frac{d\vec{g}}{ds} = |g|^{-1} \mathbf{L}_k^{\text{T}} [\mathbf{H} \cdot \vec{\nu}] \quad (6)$$

In eq 6, $\mathbf{L}_k$ is the kth eigenvector of the Hessian $\mathbf{H}$ (with the overall translation/rotation and reaction path direction projected out), and $\vec{\nu}$ is the vector along the direction of the reaction coordinate, which by definition is antiparallel to the normalized

gradient in the mass-weighted coordinate, $-\vec{g}/|g|$. The second equality in eq 6 holds because $\mathbf{L}_k$ is orthogonal to $\vec{\nu}$ and therefore annihilates another term that also contributes to $d\vec{\nu}/ds$.[57]

Although there are 14 modes in addition to the reaction coordinate, only seven make significant contributions. Four of the modes are out-of-plane bending modes and therefore do not contribute to the reaction path curvature because of symmetry considerations. The remaining modes (referred to as "path modes") are shown in Figure 9d, except for the two C−H stretches in the 3000 cm^{-1} range that are only weakly involved in the reaction. Among the eight path modes shown in Figure 9d, most make sizable contributions to the reaction path curvature (Figure 9a) except for the one at 1486 cm^{-1}. The character of this mode is a mixture of C−O and C−C stretch; because C−C stretch is not strongly involved in the reaction (especially from $s = -0.5$ to 0.0 amu$^{1/2}$ bohr), the result that it has a small curvature component is reasonable.

As discussed in Sect. III.1, the frequencies of the modes that make large contributions at the peak curvature position may be
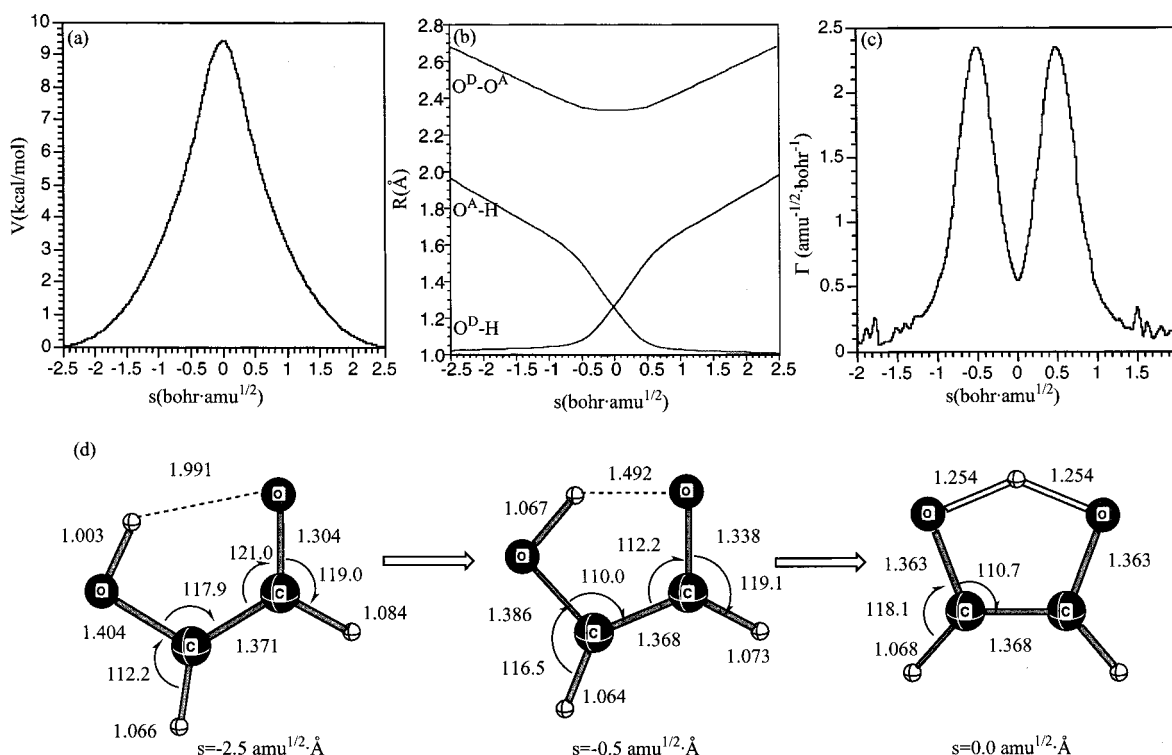
Figure 8. Properties along the minimum energy path for the proton transfer in a model enediolate in the gas phase. (a) Energy; (b) essential geometrical parameters; (c) reaction path curvature; (d) representative structures and important geometrical parameters. Distances are given in angstroms, and angles are given in degrees.
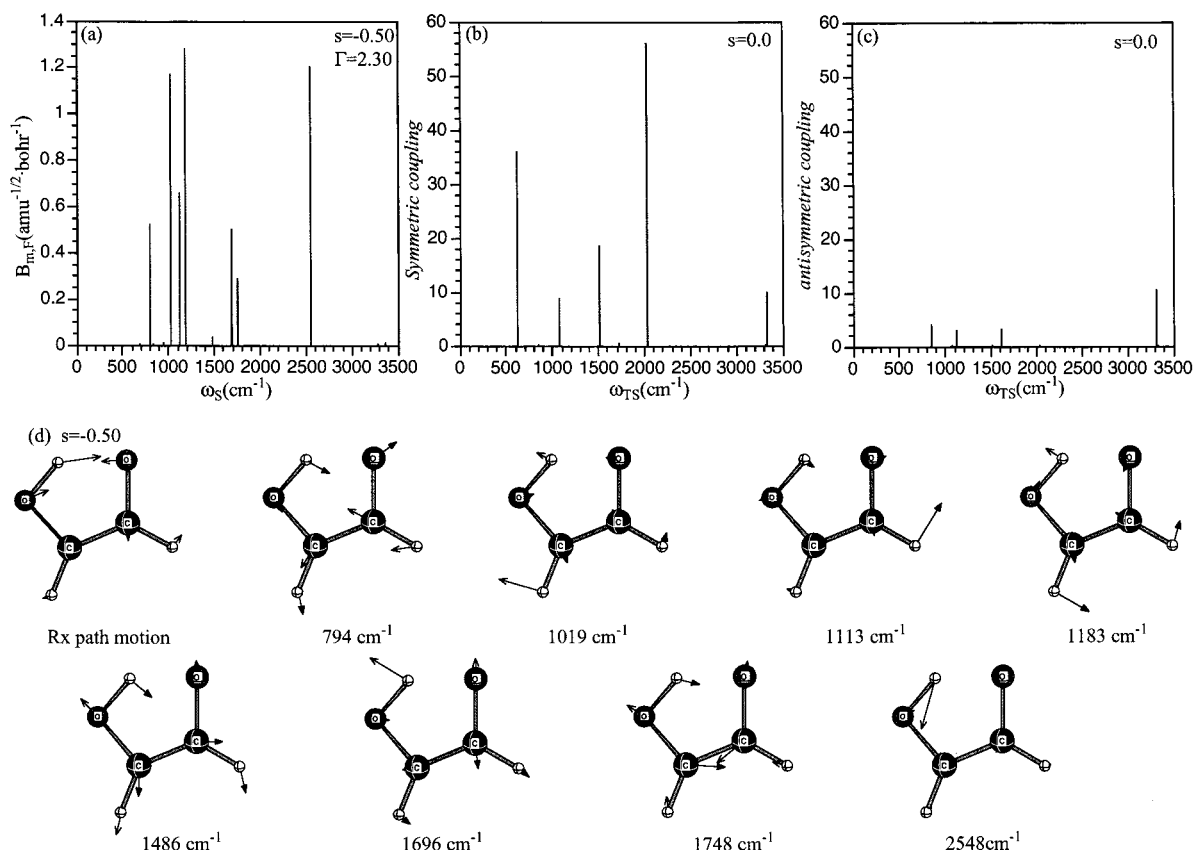

Figure 9. (a) Reaction path curvature component calculated at $s = -0.50$ amu $^{1/2}$ bohr, where the total reaction path curvature reaches a maximum, for the proton transfer in an enediolate molecule in the gas phase (see Figure 8); (b and c) Approximate symmetric and antisymmetric coupling coefficients (eq 14) for modes at the saddle point. (d) The barrier mode and selected generalized normal modes of A′ symmetry at $s = -0.50$ amu $^{1/2}$ bohr.

different from the frequencies calculated in stationary configurations. Mixing with the barrier mode and the variation of the

potential energy surface relative to stationary configurations (which was not included in the simple models discussed in

Enzyme-Catalyzed Proton Transfer Reactions

J. Phys. Chem. B, Vol. 106, No. 32, 2002 **7939**

TABLE 4: Overlap among Frequencies with Large Curvature Components and Modes at the Saddle Point in the Simple Gas Phase Enediolate Model[a]

path modes		saddle point modes		
ω (cm^{-1})	B_k,F	overlap	ω (cm^{-1})[c]	coupling strength[d]
0[b]		0.55	1365i	
		0.38	622 (s)	36.0
795	0.53	0.44	622 (s)	36.0
		0.87	853 (as)	4.0
1020	1.17	0.53	622 (s)	36.0
		0.39	853 (as)	4.0
		0.57	1079 (s)	8.8
		0.37	1131 (as)	2.9
1113	0.64	0.77	1079 (s)	8.8
		0.55	1131 (as)	2.9
1183	1.28	0.41	622 (s)	36.0
		0.74	1131 (as)	2.9
1697	0.50	0.36	1518 (s)	18.4
		0.75	1615 (as)	3.3
		0.44	2036 (s)	56.1
1748	0.30	0.96	1728 (s)	0.4
2547	1.20	0.50	1365i	
		0.33	1615 (as)	3.3
		0.78	2036 (s)	56.1

[a] The frequencies orthogonal to the reaction path were computed at $s = -0.5$amu$^{1/2}$ bohr, where the reaction path curvature has the peak value (see Figure 6). The reaction path curvature components, $B_{k,F}$, are given in amu$^{-1/2}$ bohr^{-1}. [b] The eigenvector associated with the reaction path motion at this configuration. [c] The letter in parentheses indicate the approximate character (symmetrically or antisymmetrically coupled to the proton-transfer coordinate). [d] The coupling strengths are defined in eq 14 and are given in the unit of kcal/mol Å^{-1}.

section III.1) can shift the frequencies substantially. To find out what frequencies they correspond to in the stationary structures, we calculated the overlap between those modes and the eigenvectors at the saddle point (Table 4, Figure 10). Although a similar projection can be carried out with the eigenvectors of the reactants, we chose to use the saddle point because it is of more interest; also, the structural differences between the saddle point and the configuration with largest path curvature are small. As shown in Table 4, the "path modes" at the peak curvature position have substantial overlap with a number of modes at the saddle point with different characters; the latter are shown in Figure 10 to compare with the "path modes" in Figure 9d. One important mode is the one with a frequency of 622 cm^{-1}, which is the donor–acceptor stretch (Figure 10); it has contributions from the reaction path direction (zero frequency mode at $s = -0.5$; see Table 4 and Figure 9d) and a number of medium frequency "path modes".

It is possible to determine the qualitative character of the eigenvectors at the saddle point that have large overlap with the "path modes", i.e., whether they are symmetrically ("promoting") or antisymmetrically ("demoting") coupled to the proton-transfer coordinate. To do so, we carried out the following projections

$$\Delta \bar{Y}_k^R = \Delta \bar{X}^R \cdot L_k \tag{7a}$$

$$\Delta \bar{Y}_k^P = \Delta \bar{X}^P \cdot L_k \tag{7b}$$

where $\Delta \bar{X}^R$ ($\Delta \bar{X}^P$) is the difference Cartesian coordinate vector between the reactant (product) and the saddle point in mass-weighted unit and L_k is the eigenvector for the kth mode at the saddle point. The quantity $\Delta \bar{Y}_k^R$ ($\Delta \bar{Y}_k^P$) is the position of the reactant (product) relative to the saddle point along the kth normal coordinate; $\Delta \bar{Y}_k^R$ and $\Delta \bar{Y}_k^P$ have the same signs if the
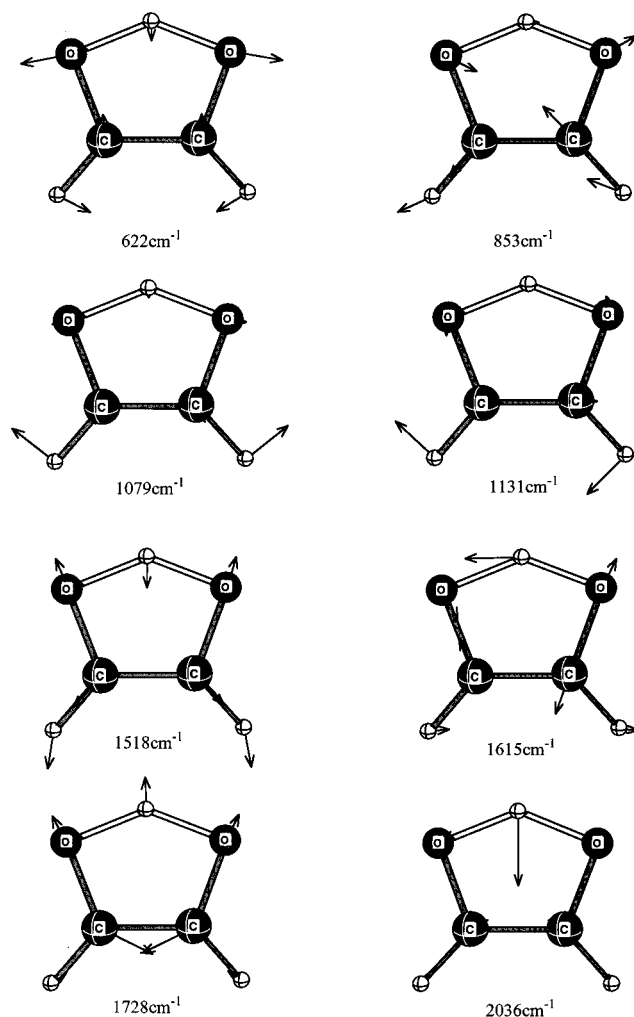

Figure 10. Normal modes at the saddle point for the proton transfer in the model enediolate species in the gas phase; these modes have large overlaps with the modes that have large curvature components (shown in Figure 9d) at $s = -0.50$amu $^{1/2}$ bohr (see also Table 4).

kth mode is symmetrically coupled to the proton-transfer coordinate, and they have different signs if the kth mode "reorganizes" in going from the reactant to the product (i.e., it is antisymmetrically coupled to the proton-transfer coordinate). For example, in the model 2D models discussed above, $\Delta \bar{Y}_k^R$ and $\Delta \bar{Y}_k^P$ equal $-C/M\Omega^2$ in the symmetric case and they equal $-c/m\omega^2$ and $c/m\omega^2$, respectively, in the antisymmetric case. Based on the discussions of tunneling and the proton-transfer rate for these 2D model potentials, the kth mode is said to be "promoting" if $\Delta \bar{Y}_k^R$ and $\Delta \bar{Y}_k^P$ have the same sign and "demoting" otherwise. In the general case, the magnitudes of $\Delta \bar{Y}_k^R$ and $\Delta \bar{Y}_k^P$ do not have to be exactly equal (e.g., in the proton transfer in TIM, see section III.3), and a symmetrization procedure can be employed

$$\Delta \bar{Y}_k^S = \frac{1}{2} |\Delta \bar{Y}_k^R + \Delta \bar{Y}_k^P| \tag{8a}$$

$$\Delta \bar{Y}_k^A = \frac{1}{2} |\Delta \bar{Y}_k^R - \Delta \bar{Y}_k^P| \tag{8b}$$

where absolute values were used because only the relative values of $\Delta \bar{Y}_k^S$ and $\Delta \bar{Y}_k^A$ are of interest. Furthermore, as seen from eq 2, the coupling coefficient between the mode and the proton-transfer coordinate is reflected by the magnitude of the displacement relative to the saddle point; for example, the minima for

the 2D model defined in section II are at $(\pm 1, -C/M\Omega^2)$ and $(\pm 1, \pm c/m\omega^2)$ for the symmetric and antisymmetric case, respectively. Therefore, we can define two approximate coupling coefficients based on $\Delta\bar{Y}_k^S$ and $\Delta\bar{Y}_k^A$ for the kth mode

$$C_k \propto \omega_k^2 \Delta\bar{Y}_k^S \qquad (9a)$$

$$c_k \propto \omega_k^2 \Delta\bar{Y}_k^A \qquad (9b)$$

where ω_k is the vibrational frequency for the kth mode. The displacement in the proton transfer coordinate, which is a constant during a given reaction and is typically 2 Å in realistic proton transfer reactions, was not explicitly included in eq 9 because only the qualitative behavior is of interest. No mass factor is necessary in eq 9 because a mass-weighted coordinate was used for $\Delta\bar{Y}_k^S$ and $\Delta\bar{Y}_k^A$. A large coupling coefficient indicates that excitation of the motion has a large effect on the energetics of proton transfer (see model potentials in section III.1).

The coupling coefficients are calculated and are shown in Figure 9b,c; their values are also included in Table 4 for modes with large overlaps with the "path modes". Because of the symmetry of the system, the modes at the saddle point are either symmetric or antisymmetric. This is not true for the "path modes", which may have large overlaps with both symmetric and antisymmetric modes. The two modes that have the largest coupling coefficients are symmetric in nature and have frequencies of 622 and 2036 cm^{-1}. The former, as discussed earlier, is the donor−acceptor stretch and is involved in a number of "path modes". The latter, which involves the symmetric O−H stretch at the saddle point (see Figure 10), is involved only in path modes of high frequency. It should be noted that all of the symmetric modes with large coupling coefficients have substantial overlaps with the "path modes", which is not necessarily true in general (see section III.3).

It is important to compare the analyses involving reaction path curvature and the coupling coefficients. The path curvature depends on the minimum-energy path, which includes displacements that have an important effect on the barrier height (e.g., the donor−acceptor stretch is an important component of the reaction coordinate close to the reactant/product). Therefore, "path modes" with large path curvatures have a direct influence on the rate mainly by modifying the tunneling contributions. However, the fact that a mode has a large curvature *implies* that the corresponding displacement makes an important contribution to the reaction coordinate, so that the energetics of proton transfer (i.e., the effective barrier) would change if that motion were not allowed. In other words, zeroing out the curvature component of a path mode does not eliminate all the effects of the corresponding motion on the proton-transfer rate; to achieve the latter, a new reaction path needs to be determined without that motion (see section III.3). Analysis of the coupling coefficients (eq 9) does not depend explicitly on the minimum-energy path, although it involves the transition state. A large coupling coefficient for a mode indicates that its excitation has a large effect on the effective energetics of the proton transfer (see discussions of model potentials in section III.1). Although it is possible to relate the coupling coefficients to the tunneling contribution with approximate instanton theories,[21,22,58] an accurate description is difficult when there is substantial asymmetry in the reaction. It is difficult, therefore, to quantify the effect of certain motion on the effective energetics of proton transfer and on the tunneling contribution with either reaction path curvature or coupling coefficients (eq 9) alone for realistic

systems, which tend to have complicated potential energy surfaces. The method of analysis we proposed here combines the two types of contributions. It appears to be a very insightful approach for analyzing the essential motions involved in reactions of large molecules (also see section III.3).

III.3. Proton Transfer in Triosephosphate Isomerase (TIM). In this section, we report some results on the rate constant for the first proton transfer in TIM (Figure 10). We will focus on the features related to the promoting modes. Other aspects of the proton transfer in TIM (e.g., isotope effects and tunneling in different environments) are described in a separate publication.[52]

The reaction is highly endothermic (>20kcal/mol) in the gas phase such that the enediolate species does not exist as a stable minimum on the potential energy surface. In TIM, the enediolate species is stabilized compared to DHAP mainly due to the charged Lys12 at the active site. Nevertheless, as shown in Figure 11a, the reaction from DHAP to EDT1 is substantially endothermic, due partly to the simplified QM used here (AM1-SRP);[59] the endothermicity is calculated to be 11.2 kcal/mol, which is significantly larger than that obtained with a higher level QM calculation (7.4 kcal/mol).[52] The reverse barrier (EDT1 → TS1) is reasonably reproduced at the AM1-SRP/CHARMM level; it is 6.1 kcal/mol in comparison to the value of 4.4 kcal/mol at the B3LYP/6-31+G(d,p)/CHARMM level. Therefore, we report only the reverse rate constant in the present work. Because tunneling is mainly determined by the potential energy surfaces close to the saddle point in the VTST framework (in contrast to certain other semiclassical models),[60] the fact that the potential energy surface drops too much after the barrier is crossed has a small effect on the results.

As shown in Figure 11b, the reaction path properties are similar to that for the model reactions described in the earlier parts of the paper. For example, the donor−hydrogen distance only starts to increase rapidly close to the saddle point, and the initial (final) stage of the reaction involves only the movement of the donor and acceptor atoms. In the enzyme environment, there are, of course, additional interactions of interest. Both His 95 and Lys 12 move significantly during the reaction, as shown in Figure 11b; that is, the O1−HNζ of Lys 12 and O2−Hε of His 95 increase by nearly 0.2 Å during the critical part of the reaction. The reaction path curvature shows two sets of peaks, one set with large curvature (>2.0 amu$^{-1/2}$ bohr^{-1}) at $s \sim \pm 0.5$ and another set with smaller peak values (~ 1 amu$^{-1/2}$ bohr^{-1}) at larger s values, -3.0 bohr and $+2.0$ amu$^{1/2}$ bohr (see below). As shown in Table 5, the position of the transition-state, as determined by variational transition-state theory,[32] is substantially different from the saddle point (by definition, $s = 0.0$) and was optimized to be at $s = -0.3$ amu$^{1/2}$ bohr along the reaction path. The tunneling contribution was found to be small; it equals a factor of 1.2 and 1.5 at the CVT-ZCT and CVT-SCT level, respectively, at 300 K. This is qualitatively consistent with the relatively small barrier height (6.1 kcal/mol) and medium barrier frequency (979i cm^{-1}); for example, a one-dimensional truncated harmonic model[61] gives a tunneling contribution of 3.1. Calculations also showed that although the absolute rate constant depends somewhat on the number of atoms allowed to move, the tunneling contribution at room-temperature varies very little (Table 5). Therefore, we used the smaller model to study the effect of fixing the donor−acceptor stretch.

In the model problems studied in section III.1, the tunneling probability was found to decrease as the Q vibration is excited (Q approaches zero). However, as also mentioned there, the

Enzyme-Catalyzed Proton Transfer Reactions

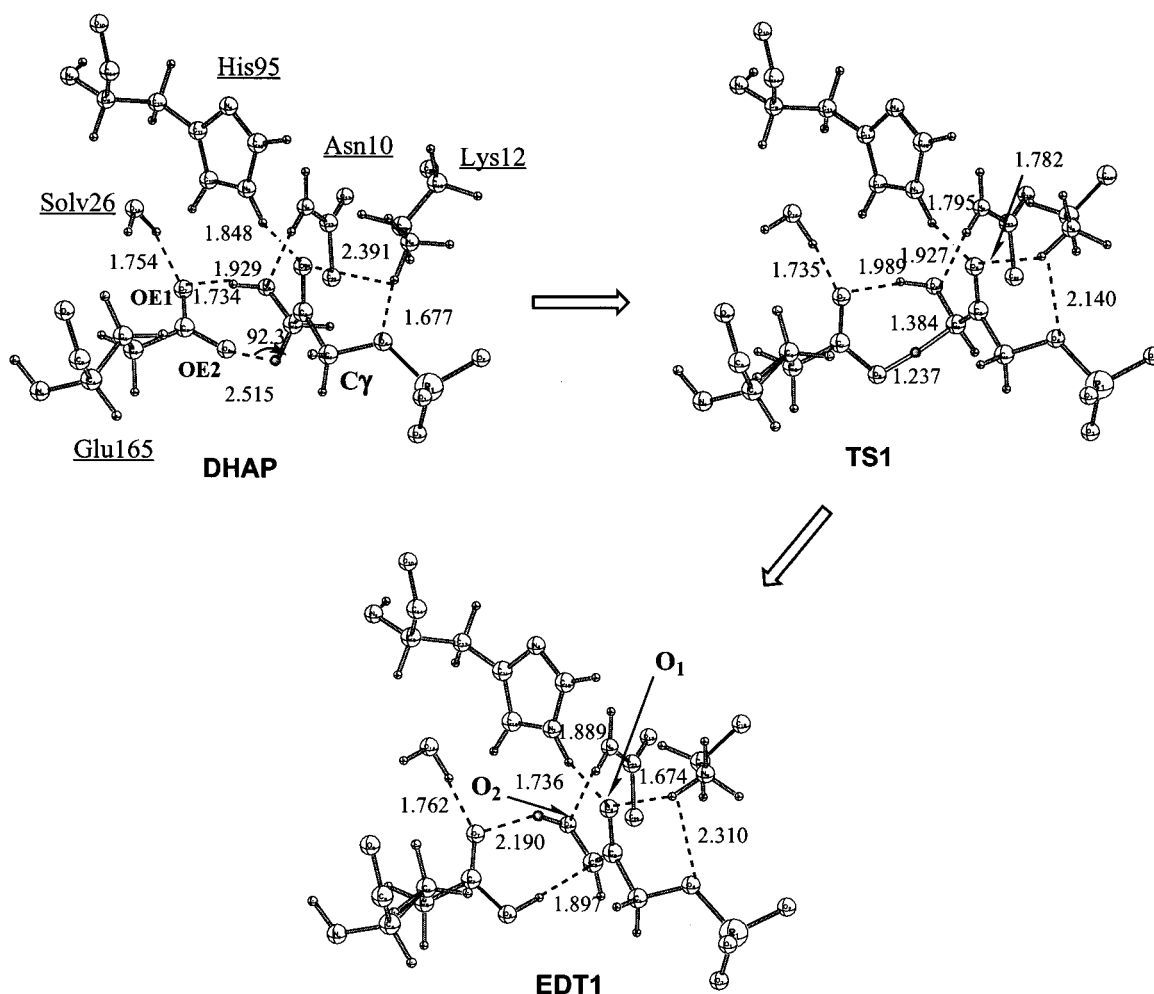*J. Phys. Chem. B, Vol. 106, No. 32, 2002* **7941**

Figure 11. Active site structures for the first proton transfer step in triosephosphate isomerase. The substrate and the side-chain of Glu165 were treated with the AM1-SRP, and the rest (only a few residues were shown) were described with the CHARMM22 force field (see the Computational Methods section).

TABLE 5: Rate Constants and Tunneling Factors for the Intermolecular Proton Transfer Reactions in TIM at 300 K[a]

	TST	CVT	CVT-ZCT	CVT-SCT
E_a/ω	6.1/924.7	(5.8/979.0)		
s^{*CVT}		$-0.31(-0.30)$		
$\log k_H(s^{-1})$	9.7 (10.4)	9.6 (10.3)	9.7 (10.4)	9.7 (10.5)
$\kappa_H^{CVT-SCT}$			1.2 (1.2)	1.5 (1.5)

[a] The values without parentheses were obtained with the large model including 445 movable atoms; those with parentheses or brackets were obtained with a smaller model including 106 movable atoms (see text). E_a is the barrier height, in kcal/mol, without zero-point energy (ZPE) correction; ω is the imaginary frequency (in cm^{-1}) at the saddle point. s^{*CVT} is the optimized position of the transition state from the canonical variational transition-state theory calculations. The SCT correction factor is defined as $k^{CVT-SCT}/k^{CVT}$.

decrease in the transfer distance due to the donor−acceptor vibration was not captured by the simple model potential. Therefore, it is interesting to examine the situation in the more realistic proton transfer in TIM being considered here. As shown in Table 6, the potential barrier has a very pronounced dependence on the donor−acceptor distance. The OE2-Cα distances at the beginning of the reaction and the transition state are 3.0 and 2.65 Å, respectively. If this distance is fixed at 3.0, 2.7, and 2.6 Å, the barrier values are 24.5, 9.2, and 3.9 kcal/mol, respectively. Furthermore, the barrier frequencies are also very different; they are 2073i, 1778i, and 1361i cm^{-1}, respectively. Correspondingly, the tunneling probabilities differ dra-

matically; they are 3.0×10^4, 36.5, and 2.1 with the donor−acceptor distances fixed at 3.0, 2.7, and 2.6 Å, respectively. Nevertheless, the rate constant for the proton transfer with the shorter donor−acceptor is much larger, by 10 orders of magnitude at 300 K (see Table 6), because of the huge difference in the barrier heights. It should be noted that it takes only 2.9 kcal/mol to bring the donor−acceptor distance from 3.0 to 2.6 Å in the EDT1 species. Therefore, the proton transfer is expected to be dominated by over-the-barrier transfer following the donor−acceptor vibration, in correspondence with Figure 11b and the small tunneling contribution given above.

Next, we examine modes that have strong coupling to the proton transfer coordinate based on the reaction path curvature. As shown in Figure 11c, the reaction path curvature exhibits two sets of peaks, one set closer to the saddle point and the other closer to the reactant/product. According to the model studies in section III.1, the inner set of peaks is due to modes that are coupled directly to the proton transfer coordinate, although they could be either "promoting" (symmetrically coupled) or "demoting" (antisymmetrically coupled). The outer set of peaks is due to modes that represent the character of the reaction path in the beginning/final stage of the reaction, i.e., motions that are relevant to the reorganization of the environment necessary for the reaction, i.e., the donor−acceptor stretch and transfer of the proton. As discussed in section III.1, only the inner set of peaks are expected to be important for the tunneling contribution; this is confirmed in the TIM model; that

TABLE 6: Rate Constants and Tunneling Factors for the Intermolecular Proton Transfer Reactions in TIM at 300 K with *the Proton Donor and Acceptor Atoms Fixed* at Difference Distances[a]

	TST	CVT	CVT-ZCT	CVT-SCT
E_a/ω	24.5/2073 (9.2/1778) [3.9/1361]			
s_*^{CVT}	−0.01 (−0.03) [+0.00]			
$\log(k_H)$	−2.5 (8.2) [11.9]	−2.5 (8.2) [11.9]	1.3 (9.4) [12.1]	2.0 (9.7) [12.2]
$\kappa_H^{CVT-SCT}$			4.9×10^3 (18.5) [1.9]	3.0×10^4 (36.5) [2.1]

[a] The values were obtained with the small model including 106 movable atoms; the positions of the proton donor (OE2 in Glu 165) and acceptor (C3 in DHAP) were fixed at 3.0, 2.7, and 2.6 for the numbers without parentheses, with parentheses and with brackets, respectively. The definitions for the quantities are the same as in Table 5.

TABLE 7: Overlap among Frequencies with Large Curvature Components and Modes at the Saddle Point in the First Proton Transfer in TIM[a]

path modes ω (cm⁻¹)	$B_{k,F}$	overlap	saddle point modes ω (cm⁻¹)[c]	coupling strength[d]
0^b		0.75	936i	
		0.30	514	5.9 (10.7)
		0.17	651	8.4 (6.8)
		0.11	918	2.6 (5.5)
		0.14	987	4.7 (7.5)
		0.13	1027	4.2 (6.4)
		0.21	1187	26.9 (3.1)
1328	0.75	0.99	1328	0.7 (0.6)
1715	0.70	0.26	936i	
		0.13	1187	26.9 (3.1)
		0.13	1333	25.1 (22.4)
		0.22	1618	3.1 (5.0)
		0.45	1623	3.8 (5.7)
		0.16	1628	0.8 (1.6)
		0.21	1712	(0.0)
		0.57	1717	0.1 (0.0)
		0.18	1726	0.0 (1.7)
		0.11	1766	0.6 (0.3)
		0.23	1921	1.3 (8.9)
		0.19	1978	0.8 (2.1)
2093	0.69	0.30	936i	
		0.12	1187	26.9 (3.1)
		0.18	1920	1.3 (8.9)
		0.88	1978	0.8 (2.1)
1719	0.58	0.18	936i	
		0.15	1618	3.1 (5.0)
		0.31	1623	3.8 (5.7)
		0.11	1628	0.8 (1.6)
		0.81	1717	0.1 (0.0)
		0.22	1726	0.0 (1.7)
		0.16	1920	1.3 (8.9)
		0.13	1978	0.8 (2.1)
1520	0.55	0.18	936i	
		0.13	1187	26.9 (3.1)
		0.14	1333	25.1 (22.4)
		0.18	1410	21.0 (22.4)

path modes ω (cm⁻¹)	$B_{k,F}$	overlap	saddle point modes ω (cm⁻¹)[c]	coupling strength[d]
1520	0.55	0.25	1411	29.3 (31.3)
		0.13	1417	10.5 (12.0)
		0.15	1417	9.9 (11.3)
		0.11	1418	8.0 (9.4)
		0.41	1522	1.0 (0.4)
		0.35	1525	4.1 (0.3)
		0.39	1528	12.6 (0.3)
		0.20	1619	3.1 (5.0)
		0.34	1623	3.8 (5.7)
		0.11	1627	0.8 (1.6)
		0.15	1978	0.8 (2.1)
1328	0.46	0.23	936i	
		0.12	987	4.7 (7.5)
		0.10	1027	4.2 (6.4)
		0.25	1187	26.9 (3.1)
		0.31	1330	4.3 (4.0)
		0.61	1333	25.1 (22.4)
		0.20	1335	4.9 (4.2)
		0.20	1410	21.0 (22.4)
		0.30	1411	29.3 (31.3)
		0.11	1417	10.5 (12.0)
		0.13	1417	9.9 (11.3)
		0.12	1621	3.8 (5.7)
552	0.46	0.12	511	1.1 (2.7)
		0.59	514	5.9 (10.7)
		0.19	547	0.4 (0.1)
		0.12	548	0.4 (0.0)
		0.22	550	0.2 (0.2)
		0.35	553	0.1 (0.1)
		0.22	555	0.2 (0.1)
		0.28	599	11.8 (4.5)
		0.12	644	2.3 (1.8)
		0.17	651	8.4 (6.8)
		0.14	677	3.4 (7.4)
		0.11	691	4.5 (5.8)

[a] The frequencies orthogonal to the reaction path were computed at $s = -0.32$ amu$^{1/2}$ bohr, where the reaction path curvature has the peak value (see Figure 10). The reaction path curvature components, $B_{k,F}$, are given in amu$^{-1/2}$ bohr^{-1}. [b] The eigenvector associated with the reaction path motion at this configuration. [c] The letter in parentheses indicate the approximate character (symmetrically or antisymmetrically coupled to the proton-transfer coordinate). [d] The coupling strengths are defined in eq 14, and are given in the unit of kcal/mol Å^{-1}. The values without parentheses are the approximate symmetric components, and the values with parentheses are the approximate antisymmetric components.

is, zeroing out the outer-peaks in the reaction path curvature gave virtually identical SCT rate constants. Therefore, we focus on the inner set of peaks in the following analysis of important motions in TIM. However, as discussed in section III.2., leaving out the curvature components does not eliminate all of the effects of the corresponding motions; the fact that these modes have a sizable curvature component indicates that they are an essential part of the (initial/final) reaction coordinate and therefore modulate the energetics of proton transfer. They do not, however, contribute directly to proton tunneling.

Following the analysis procedure in section III.2, the reaction path curvature at the inner peak positions ($s = -0.31$ amu$^{1/2}$ bohr) was decomposed into contribution from modes orthogonal

to the reaction path (Figure 11d); the overlaps between the "path modes" and the eigenvectors at the saddle point were calculated (Table 7). The effective coupling coefficients (eq 9) were also computed for the eigenvectors ("essential modes") with large overlaps (Figure 11e,f and Table 8). The normal modes at the saddle points having the largest coupling coefficients are plotted in Figure 12.

As shown in Table 7, the "path modes" with large curvature components typically have substantial overlap with many modes at the saddle point ("essential modes"); however, the situation is more complex than that found in the simple gas-phase model discussed in section III.2. The barrier mode (936i) has large overlaps with many "path modes" with relatively high fre-

Enzyme-Catalyzed Proton Transfer Reactions

J. Phys. Chem. B, Vol. 106, No. 32, 2002 **7943**

TABLE 8: Characters of Normal Modes at the Saddle Point that Have Large Overlaps to the Modes with Large Reaction Path Curvature Components for the First Proton Transfer in TIM[a]

ω, R_i^I,R_i^{II},C	resi.	dist.	contri.	ω, R_i^I,R_i^{II},C	resi.	dist.	contri.
936i	Subs		0.89	1333	Subs		0.87
5.5	E165	5.8	0.09	13.6	C126	9.5	0.03
1.2	K12	5.9	0.01	1.3	T75B	8.7	0.03
	H95	7.3	0.01	25.1 (22.4)	L230	5.6	0.03
	W26	6.3	0.01		E165	5.8	0.03
514	E165	5.8	0.45	1410	A212	7.0	0.56
30.2	Subs		0.41	15.4	Subs		0.31
2.7	W27	8.2	0.03	2.4	S211	6.8	0.09
5.9 (10.7)	W245	6.0	0.03	21.0 (22.4)	E165	5.8	0.02
	W26	6.3	0.02		V231	5.9	0.01
599	Subs		0.52	1411	Subs		0.60
28.9	E165	5.8	0.35	11.4	A212	7.0	0.29
2.6	P166	9.1	0.02	2.2	S211	6.8	0.05
11.8 (4.5)	W	8.6	0.02	29.3 (31.3)	E165	5.8	0.04
	S235	8.4	0.01		N8	5.5	0.01
1187	Subs		0.94	1528	Subs		0.84
5.4	E165	5.8	0.02	2.6	H95	7.3	0.10
1.1	L230	5.6	0.01	1.4	S96	8.4	0.05
26.9 (3.1)	F229	10.0	0.01	12.6 (0.3)	E165	5.8	0.01
	V231	5.9	0.01		G232	3.9	0.01
1192	Subs		0.97	1417	I170	4.8	0.34
3.5	H95	7.3	0.01	21.7	Subs		0.33
1.1	K12	5.9	0.01	3.6	E165	5.8	0.24
13.2 (3.0)	E165	5.8	0.01	10.5 (12.0)	P166	9.1	0.06
	I170	4.8	0.01		H95	7.3	0.02

[a] Distances are defined as the center of geometry distances between the residues (*including* the main chain atoms) and the substrate. The R_i's are the participation ratios (see eq 4) for the ith mode; for the definition of the coupling coefficients (C), see the footnote of Table 7. [b] The contribution of each residue is defined as the term after the furst summation in eq 4b.

quency, representing the fact that the character of the reaction coordinate is changing rapidly at the peak curvature position ($s = -0.3$). Most essential modes have large coupling coefficients, although there are exceptions (e.g., the 1328 cm^{-1} mode has a large curvature component but relatively small coupling coefficients). It should be noted that, similar to the situation in the gas phase model, the analysis based on the reaction path curvature (which has direct effect on the tunneling contribution in the VTST framework) captured most of the modes with large symmetric/antisymmetric coupling coefficients. Because the reaction is far from being symmetric (see Figure 9a), usually both the symmetric and antisymmetric coupling coefficients are substantial (e.g., modes at 1333 and 1410 cm^{-1}; see Table 7). Two notable exceptions are the modes with frequencies of 1187 and 1528 cm^{-1}, which are dominated by the symmetric component.

As shown in Table 8 and Figure 12, most essential modes are rather localized and involve mainly the substrate and Glu165 (which contains the reacting group), as reflected by the participation ratios; the barrier mode has a similar character. The donor and acceptor atoms are heavily involved in many modes, especially those at low frequencies (e.g., 514 and 598 cm^{-1}). Other atoms in the substrate/Glu165 can also be involved; for example, $C_\alpha-O_\alpha$ and $C_\gamma-O^P$ stretches and $O\epsilon1-C\epsilon-O\epsilon2$ bending are heavily involved in the modes at 1192 and 598 cm^{-1}, respectively. In some modes, other nearby residues also make notable contributions; for example, Ala 212 and Ile 170 have sizable components in the modes at 1410 and 1417 cm^{-1}, respectively. A residue from the other subunit on the dimer interface, Thr 75B, also has a small component in the mode at 1333 cm^{-1}. This residue has been shown to contribute significantly to the reaction.[59,62]

IV. Concluding Discussion: Promoting Modes, Demoting Modes, and Proton Transfer in Enzymes

We have studied a number of proton transfer reactions with analytical model or semiempirical potential functions using variational transition-state theory. An effort was made to clarify the identity of modes (e.g., "promoting modes") that can influence the rate constant of proton transfer reactions, especially in the context of enzyme catalysis.

VTST calculations on model potentials illustrated, as suggested in earlier work,[10,23,25] that the effect of a vibrational mode on the rate constant depends on the symmetry of the coupling between this mode and the proton-transfer coordinate. Modes (Q) that are symmetrically coupled to the proton-transfer coordinate have promoting effects relative to the *uncoupled* reaction; i.e., the couplings increase the rate constant. The meaning and cause of the promotion effect depends on the system of reference and temperature (also see the Supporting Information). At room temperature, the increase in the rate constant is due mainly to the lowering of the effective barrier along the proton-transfer coordinate, relative to the uncoupled system and the proton transfer with Q fixed at its equilibrium value. The promoting effect is, therefore, primarily *classical*. In fact, the *contribution of tunneling* becomes smaller at vibrationally excited Q. At low temperatures, the rate increases because the contribution of tunneling (which is dominated by deep tunneling with little excitation of Q corresponding to severe "corner-cutting" dynamics) is larger relative to the uncoupled reaction (which does not involve corner-cutting), as a result of the increased effective frequency of the barrier. Thus, for the "promoting effect" to take place, excitation of the Q vibration is essential *only* at room temperature. The antisymmetric mode (x), by contrast, has "demoting effects", relative to uncoupled proton transfer. The coupling lowers the effective barrier frequency, which leads to a decrease of tunneling. More importantly, the antisymmetric coupling gives rise to asymmetry in the effective potential along the proton transfer coordinate and, therefore, restricts tunneling to occur effectively only at excited x (e.g., x = 0 in the 2D case) at all temperatures. In other words, vibrational excitation of the antisymmetric modes is also essential for the proton transfer; antisymmetric coupling lowers the rate less severely if the x vibration is excited because then the effective 1D potential becomes symmetric and tunneling can occur as efficiently as in the uncoupled/symmetric 2D case, except for the effect of the lower barrier frequency.

The calculations demonstrated that the coupling between the proton-transfer coordinate and the orthogonal modes (Q or x) has a clear signature in the reaction path curvature. Therefore, it is possible to identify motions that are important to the reaction (e.g., those catalyzed by enzymes) by examining modes with large reaction path curvature components, and it is straightforward to distinguish their qualitative characters, i.e., symmetric ("promoting") or antisymmetric ("demoting") modes. This was demonstrated with both the simple gas-phase enediolate system and the first proton-transfer step in TIM. The procedure is complementary to the proposal of Schwartz et al.[25a] (who examined the spectral density as a function of the proton-transfer coordinate) and has the advantage that the atomic contributions can be characterized for realistic systems which have complicated potential energy surfaces. The calculations on the proton transfer in TIM demonstrated that the reaction is coupled to a large number of vibrational motions in the active site. One of these modes, as expected, is the donor–acceptor stretch, which modulates the effective barrier for the proton transfer and also the magnitude of the tunneling. Corresponding to the proton-
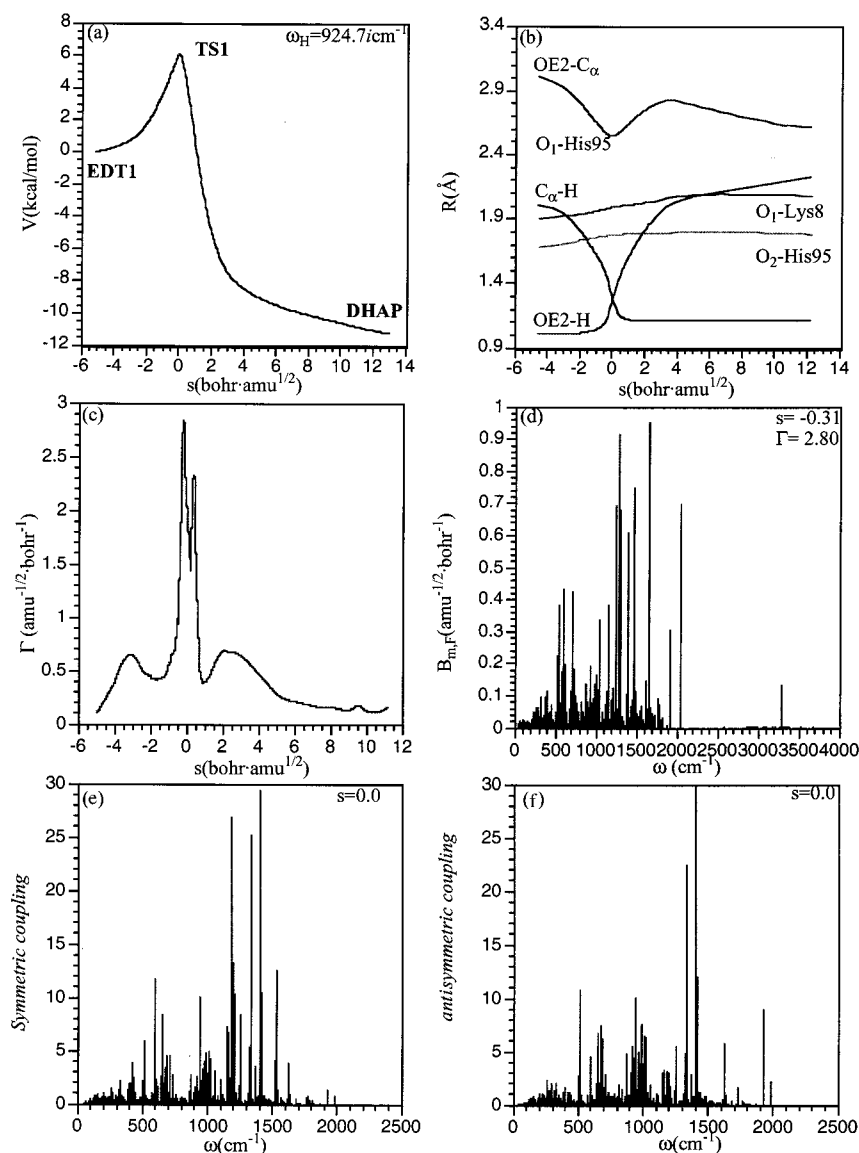
Figure 12. (a) Energetics, (b) important geometrical parameters, and (c) reaction path curvature along the reaction coordinate for the first proton-transfer step in triosephosphate isomerase; (d) Normal mode decomposition of the reaction path curvature at the peak curvature position ($s = -0.31$ amu$^{1/2}$ bohr). (e and f) Approximate symmetric and asymmetric coupling coefficients (eq 14) for modes at the saddle point.

transfer calculations with the model potentials, it was found that tunneling becomes more important at large donor−acceptor distances and that the enhancement of the transfer rate when the donor−acceptor stretch is excited is largely a classical effect (i.e., the effective barrier is lowered). There are other modes that are symmetrically or antisymmetrically coupled to the proton-transfer coordinate, such as those involving nearby residues (Ala 212 and Ile 170). Their effect is to prepare the enzyme environment by lowering the effective proton-transfer barrier.

It should be noted that an assumption made in the above analysis is that energy is quickly randomized between the Q/q and x degrees of freedom during the time-scale of the overall reaction; that is, we assume that there is substantial coupling between the Q/x and q and thus energy can flow rapidly between them with a rate much faster than the motion along the reaction coordinate.[65a] This is likely to hold for highly anharmonic systems like enzymes and typical proton transfer reactions that have a barrier on the order of 10 kcal/mol. The "promoting" and "demoting" effects described are essentially equilibrium (thermodynamical) effects; that is, the vibrational excitation of

those modes modifies the shape and height of the effective proton-transfer barrier. In principle, these modes can also have a substantial nonequilibrium (dynamical) contribution,[63−65] which is characterized by the transmission coefficient. For the vibrational effect on the transmission coefficient, the energy randomization may not be fast compared to the barrier-crossing event. For example, the barrier-crossing time for the proton transfer in TIM was found to be 30 fs,[64] much faster than the expected rate of energy redistribution, which is expected to be slower than the frequency of the modes involved (around 300 cm^{-1} in TIM[64]). Thus, proton tunneling/transfer at nonoptimal (instantaneous) environmental configuration (e.g., unexcited x) may contribute to the dynamical transmission coefficient.[66] However, it should be noted that the magnitude of the dynamical effect is generally small at room temperature; it was found to be about a factor of 2 for the first proton-transfer step in triosephosphate isomerase.[64] When the current work was essentially finished, Billeter et al.[20] reported a transmission coefficient very close to one (0.947) for the hydride transfer in liver alcohol dehydrogenase and a slightly smaller value (0.80) for dihydrofolate reductase.[67]
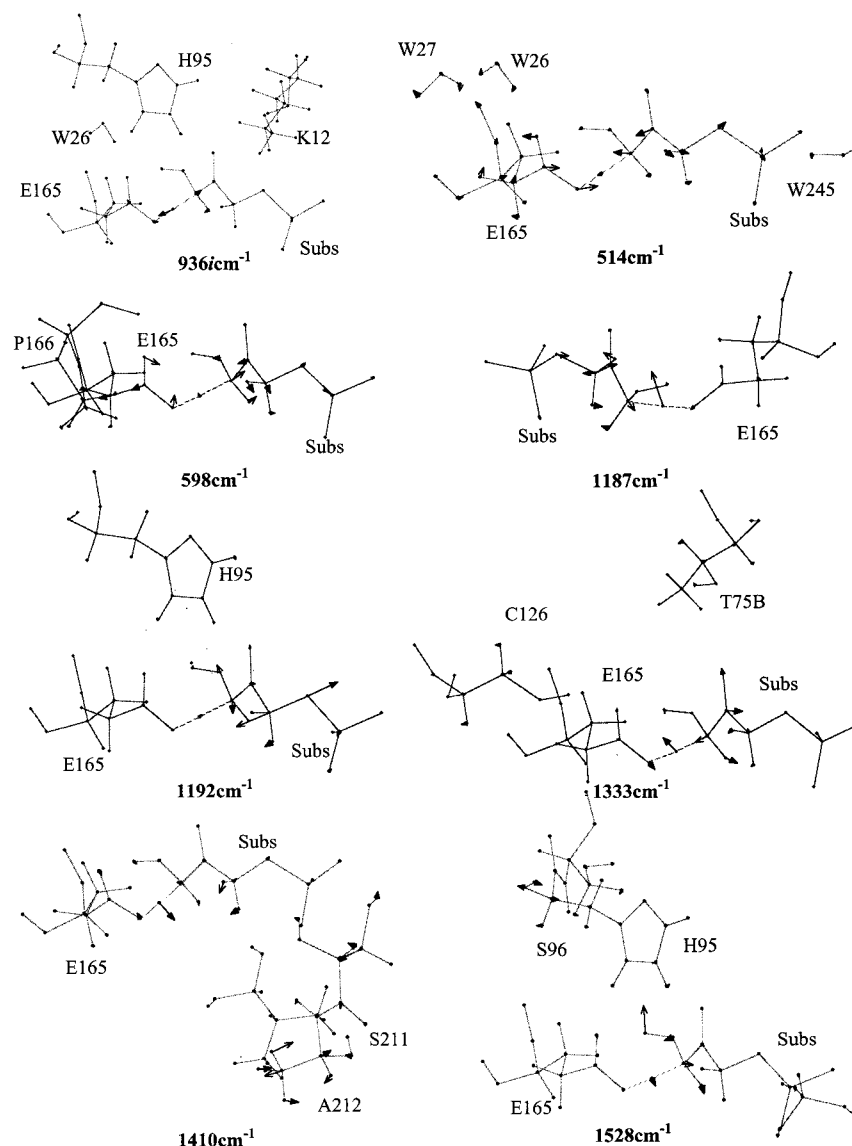
Enzyme-Catalyzed Proton Transfer Reactions

J. Phys. Chem. B, Vol. 106, No. 32, 2002 **7945**

Figure 13. Normal modes at the saddle point for the first proton-transfer step in triosephosphate isomerase; these modes have large overlaps with the modes that have large curvature components. For the overlaps between the path modes and essential modes, the approximate coupling coefficients, and their characters, see Tables 7 and 8.

It has been stated in the literature that the apparent barrier for proton/hydride transfer reactions is not determined by the potential energy function for donor−hydrogen cleavage because the positions of heavy atoms (particularly the donor−acceptor distance) are critical.[23] This statement does not mean that the "reorganization" of the environment cannot be captured in a minimum energy path (MEP)-based description, because the potential along MEP is *not* just that corresponding to the donor−hydrogen cleavage coordinate and the necessary "reorganization" effect (i.e., the decrease of the donor−acceptor distance) is explicitly included. Therefore, variational transition-state theory, which is based on the potential surface around the MEP, is able to capture the effect of "environmental" vibrations on the proton-transfer rate constants. In the just published analysis of Kiefer and Hynes on adiabatic proton-transfer reactions,[26] the solvent polarization and proton donor−acceptor vibration was used to define the reaction coordinate. The proton motion, therefore, is transverse to the reaction coordinate. It was then suggested that this transverse character of proton motion is critical to the contribution from zero-point energy (ZPE) change to the activation free energy, and it was further commented that no ZPE contribution can arise in "traditional approaches" in

which proton motion is considered as the reaction coordinate. We emphasize again that the MEP approach does not assume that proton displacement, per se, is the reaction coordinate. Because the initial and final segments of the MEP are dominated by changes in environmental variables, such as the donor−acceptor stretch, to which the proton motion is indeed transverse, ZPE makes a major contribution to the activation barrier in the present models.

On the basis of the above findings, we comment briefly on the intriguing experimental results for the thermophillic ADH obtained by Klinman and co-workers,[14a] although the lack of an X-ray structure of the enzyme prevents a more complete analysis. The major findings from the kinetic measurements in ref 14a are as follows: (1) the apparent activation enthalpy increases dramatically from 14.6 kcal/mol around the optimal temperature for the enzyme (30−65 °C) to 23.6 kcal/mol at lower temperatures (0−30 °C); (2) the H/D kinetic isotope stays around 2.5 in the former regime and has a strong temperature dependence in the latter; (3) the secondary SSE is much larger at high temperatures (>10 at 65 °C) than that at lower temperatures (∼5 at 0 °C), although there is substantial uncertainty in the measured values; (4) the Arrhenius plot

(logarithm of rate constant vs the reciprocal temperature) has a convex form (instead of the concave behavior typically observed), and the slope changes around 30 °C; (5) the Arrhenius parameters at higher temperature is also substantially larger; e.g., A_H/A_T is 4.3 (± 0.6) and 0.26 (± 0.23) for 30−65 °C and 5−30 °C, respectively. On the basis of observation 1, it was suggested that the flexibility of the enzyme, which has been observed to decrease for thermophiles at temperatures far from the optimal value,[18,68] plays an important role in determining the barrier for the hydride transfer. H/D exchange measurements on the thermophillic ADH support the suggestion that the structure is less flexible at temperatures below 30 °C.[69] Also, observations 3 and 5 were interpreted as suggesting that tunneling makes a larger contribution at higher temperatures than lower temperatures, which seems counterintuitive, as the authors realized.

Several of the observations for the thermophillic ADH are in accord with expectations and the calculations reported here. For example, observation 2 on the temperature dependence of the H/D kinetic isotope effect is normal; that is, it increases as the temperature decreases as expected (e.g., see Table 2 or Figure 4 for the 1D and 2D models). It was suggested in ref 25b that it is puzzling that the H/D kinetic isotope effect is temperature-independent between 30 and 65 °C; the experimental measurements (Figure 4 in ref 14a), however, have considerable uncertainties. Our calculations on TIM,[52] horse liver alcohol dehydrogenase,[34] and the systems studied in the current work all demonstrate that there is no necessary correlation between the magnitude of the tunneling contribution and the SSE. In fact, the secondary SSE can become very large because the logarithm of the secondary D/T kinetic isotope effect, which is the denominator in the definition of the SSE, becomes very small at high temperatures, as expected. The convex behavior for the Arrhenius parameters (observations 4 and 5) also do not necessarily suggest that tunneling makes a larger contribution at higher temperature; rather, it is likely to be directly related to the fact that the effective barrier is substantially higher at low temperatures (observation 1).

Given the above, the most intriguing and key aspect of the thermophillic ADH is observation 1, i.e., the increase of the barrier by 9 kcal/mol within a relatively narrow temperature range. It was suggested that the dramatic change in the barrier arises in part from the increased reorganization energy at low temperature due to the decrease in the flexibility of the protein. From the calculations we (and others) have made, it is unlikely that the flexibility of the protein would alter the barrier for the hydride transfer by 9 kcal/mol around 30 °C. For example, in a previous study on the mesophillic horse liver alcohol dehydrogenase,[34] the classical potential of mean force (PMF) for the hydride transfer reaction was calculated at both 200 and 300 K; several calculations were also carried out with the environment and the active site (51 atoms) maintained at different temperatures (100−300 K). The results indicate that, although the flexibility of the protein does have an effect on the PMF for the hydride transfer, the effect is less than 1 kcal/mol between 200 and 300 K (also see below). The classical PMF was expected to be meaningful because VTST calculations found a very small contribution from tunneling at room temperature.[34] It is interesting to note also that for the enzyme glutamate dehydrogenase the activation energy was found to be essentially constant between 180 and 280 K; the lowest temperature is below the dynamic glass transition.[70] A possible explanation of these perplexing results is that a structural or mechanistic change occurs 30 °C in the thermophillic ADH.

Combining the results for the models with simple potential energy functions and the model for the proton transfer in TIM with a more realistic potential, it is clear that specific vibrational motions (both symmetric and antisymmetric modes!), which are rather localized to atoms in the active site, are important for the proton transfer in enzymes. Restricting the vibrational excitation of these modes would modify the effective proton-transfer barrier and therefore influence the rate of transfer through both classical/quantum mechanical and equilibrium/dynamical effects. An interesting question is whether these vibrations are "absent" in solution, and therefore, the reaction will benefit from the existence of these modes in the enzyme environment. For an intramolecular proton transfer, comparison between the reaction in solution and in the enzyme found rather similar behavior in the reaction path curvature and its normal mode decomposition.[52] This is a somewhat special case, however, because the transfer is within the substrate, and TIM actually has an anticatalytic effect on the reaction.[59] Detailed theoretical or experimental analyses on the temperature dependence of a reaction in an enzyme relative to that in solution would be of great value in answering this question.

Supporting Information Available: Analyses on the effects of a symmetrically or asymmetrically coupled mode on the proton transfer rate constant. This material is available free of charge via the Internet at http://pubs.acs.org.

References and Notes

(1) (a) Fersht, A. *Structure and mechanism in protein science*; W. H. Freeman and Company: New York, 1999. (b) Jencks, W. P. *Catalysis in Chemistry and Biology*; Dover: New York, 1987.

(2) For recent analyses, see, for example: (a) Wu, N.; Mo, Y. R.; Gao, J. L.; Pai, E. F. *Proc. Natl. Acad. Sci. U.S.A.* **2000**, *97*, 2017. (b) Warshel, A.; Strajbl, M.; Villa, J.; Florian, J. *Biochem*. **2000**, *39*, 14728.

(3) See, for example: (a) Warshel, A. *J. Biol. Chem*. **1998**, *273*, 27035. (b) Cannon, W. R.; Benkovic, S. J. *J. Biol. Chem*. **1998**, *273*, 26257.

(4) See, for example: Villa, J.; Strajbl, M.; Glennon, T. M.; Sham, Y. Y.; Chu, Z. T.; Warshel, A. *Proc. Natl. Acad. Sci. U.S.A.* **2000**, *97*, 11899.

(5) See, for example: Cleland, W. W.; Frey, P. A.; Gerlt, J. A. *J. Biol. Chem.* **1998**, *273*, 25529.

(6) (a) Karplus, M.; McCammon, J. A. *Nature* **1979**, *277*, 578. (b) Welch, G. R.; Somogyi, B.; Damjanovich, *S. Prog. Biophys.*, *Mol. Biol*. **1982**, *39*, 109.

(7) For a recent enthusiastic discussion, see, for example: Wilson, E. K. *Chem. Eng. News* **2000**, *78*, 42.

(8) We note that in theoretical analyses, "dynamics" typically refers to the properties of the environment that influence the transmission coefficient. In the experimental community, however, "dynamics" is often used as a general term to describe the motion of the protein. For discussions of this point, see, for example, refs 20, 34, and 65a.

(9) Bruice, T. C.; Benkovic, S. J. *Biochem*. **2000**, *39*, 6267.

(10) Borgis, D.; Hynes, J. T. In *The Enzyme Catalysis Process*; Cooper, A., Houben, J., Chien, L., Eds.; Plenum: New York, 1989; p 293.

(11) Agmon, N.; Hopfield, J. J. *J. Chem. Phys.* **1983**, *79*, 2042.

(12) For a recent review, see: Kohen, A.; Klinman, J. *Acc. Chem. Res.* **2000**, *31*, 397.

(13) (a) Alston, W. C.; Manska, M.; Murray, C. J. *Biochem.* **1996**, *35*, 12873. (b) Suteliffe, M. J.; Scrutton, N. S. *Trends Biol. Sci.* **2000**, *25*, 405.

(14) (a) Kohen, A.; Cannio, R.; Bartolucci, S.; Klinman, J. P. *Nature* **1999**, *399*, 496. (b) Cha, Y.; Murray, C. J.; Klinman, J. P. *Science* **1989**, *243*, 1325. (c) Bahnson, B. J.; Colby, T. D.; Chin, K. J.; Goldstein, B. M.; Klinman, J. P. *Proc. Natl. Acad. Sci. U.S.A.* **1997**, *94*, 12797.

(15) Grant, K. L.; Klinman, J. P. *Biochemistry* **1989**, *28*, 6597.

(16) Kohen, A.; Jonsson, T.; Klinman, J. P. *Biochemistry* **1997**, *36*, 2603.

(17) (a) Glickman, M. H.; Klinman, J. P. *Biochemistry* **1995**, *34*, 14077. (b) Glickman, M. H.; Klinman, J. P. *J. Am. Chem. Soc.* **1994**, *116*, 793.

(18) Zavodszky, P.; Kardos, J.; Svingor, J.; Petsko, G. A. *Proc. Natl. Acad. Sci. U.S.A.* **1998**, *95*, 7406.

(19) Rudd, P. M.; Joao, H. C.; Coghill, E.; Fiten, P.; Saunders, M. R.; Opdenakker, G.; Dwek, R. A. *Biochem.* **1994**, *33*, 17.

(20) Billeter, S. R.; Webb, S. P.; Agarwal, P. K.; Iordanov, T.; Hammes-Schiffer, S. *J. Am. Chem. Soc.* **2001**, *123*, 11262.

(21) (a) Benderskii, V. A.; Markarov, D. E.; Grinevich, P. *Chem. Phys.* **1993**, *170*, 275. (b) Benderskii, V. A.; Markarov, D. E.; Wight, C. A. *Adv. Chem. Phys.*; John Wiley & Sons: New York, 1994.

(22) Miller, W. H. *J. Chem. Phys.* **1975**, *62*, 1899.

(23) (a) Borgis, D.; Hynes, J. T. *J. Chem. Phys.* **1991**, *94*, 3619. (b) Borgis, D.; Hynes, J. T. *J. Phys. Chem.* **1996**, *100*, 1118.

(24) Suarez, A.; Silbey, R. *J. Chem. Phys.* **1991**, *94*, 4809.

(25) (a) Caratzoulas, S.; Schwartz, S. D. *J. Chem. Phys.* **2001**, *114*, 2910. (b) Antoniou, D.; Schwartz, S. D. *J. Phys. Chem. B* **2001**, *105*, 5553. (c) Antoniou, D.; Schwartz, S. D. *J. Chem. Phys.* **1998**, *108*, 3620. (d) Antoniou, D.; Schwartz, S. D. *Proc. Natl. Acad. Sci. U.S.A.* **1997**, *94*, 12360.

(26) (a) Kiefer, P. M.; Hynes, J. T. *J. Phys. Chem. A* **2002**, *106*, 1834. (b) Kiefer, P. M.; Hynes, J. T. *J. Phys. Chem. A* **2002**, *106*, 1850.

(27) For a recent discussion in the context of VTST, see: Schenter, G. K.; Garrett, B. C.; Truhlar, D. G. *J. Phys. Chem. B* **2001**, *105*, 9672.

(28) (a) Caldeira, A. O.; Leggett, A. J. *Phys. Rev. Lett.* **1981**, *46*, 211. (b) Caldeira, A. O.; Leggett, A. J. *Ann. Phys.* **1983**, *149*, 374. (c) Leggett, A. J.; Chakravarty, S.; Dorsey, A. T.; Fisher, M. P. A.; Garg, A.; Zwerger, W. *Rev. Mod. Phys.* **1987**, *59*, 1.

(29) Wolynes, P. *Phys. Rev. Lett.* **1981**, *47*, 468.

(30) Topaler, M.; Makri, N. *J. Chem. Phys.* **1994**, *101*, 7500.

(31) See, for example: (a) Hänggi, P.; Pollak, E.; Grabert, H. *The Quantum Kramers Problem*; University of Augsburg: FRG, 1989. (b) Pollak, E.; Grabert, H.; Hänggi, P. *J. Chem. Phys.* **1989**, *91*, 4073.

(32) (a) For a recent review, see: Truhlar, D. G.; Garrett, B. C.; Klippenstein, S. J. *J. Phys. Chem.* **1996**, *100*, 12771. (b) Truhlar, D. G.; Isaacson, A. D.; Garrett, B. C. In *Theory of Chemical Reaction Dynamics*; Bear, M., Ed.; CRC Press: Boca Raton, FL, 1985; Vol. 4, p 65.

(33) See, for example: Garrett, B. C.; Joseph, T.; Truong, T. N.; Truhlar, D. G. *Chem. Phys.* **1989**, *136*, 271.

(34) Cui, Q.; Elstner, M.; Karplus, M. *J. Phys. Chem. B* **2002**, *106*, 2721.

(35) Marcus, R. A. *J. Phys. Chem.* **1968**, *72*, 891.

(36) (a) Marcus, R. A. *J. Chem. Phys.* **1956**, *24*, 966. (b) Marcus, R. A. *Annu. Rev. Phys. Chem.* **1964**, *15*, 155.

(37) For a recent discussion, see, for example: Webb, S. P.; Agarwal, P. K.; Hammes-Schiffer, S. *J. Phys. Chem. B*, **2000**, *104*, 8884.

(38) Gehlen, J. N.; Chandler, D.; Kim, H. J.; Hynes, J. T. *J. Phys. Chem.* **1992**, *96*, 1748.

(39) Cui, Q.; Brumer, Y.; Reichman, D.; Karplus, M. not published.

(40) Brooks, C. L., III.; Karplus, M. *J. Mol. Biol.* **1989**, *208*, 159.

(41) Field, M.; Bash, P. A.; Karplus, M. *J. Comput. Chem.* **1990**, *11*, 700.

(42) Gonzalez-Lafont, A.; Truong, T. N.; Truhlar, D. G. *J. Phys. Chem.* **1991**, *95*, 4618.

(43) See, for example: Cho, M.; Fleming, G.; Saito, S.; Ohmine, I.; Stratt, R. M. *J. Chem. Phys.* **1994**, *100*, 6672.

(44) Sagnella, D. E.; Straub, J. E. *Biophys. J.* **1999**, *77*, 70.

(45) See for example: Marcus, R. A.; Coltrin, M. E. *J. Chem. Phys.* **1977**, *67*, 2609.

(46) Miller, W. H.; Handy, N. C.; Adams, J. E. *J. Chem. Phys.* **1980**, *72*, 99.

(47) Garrett, B. C.; Joseph, T.; Truong, T. N.; Truhlar, D. G. *Chem. Phys.* **1989**, *136*, 271.

(48) For examples, see: (a) Mielke, S. L.; Allison, T. C.; Truhlar, D. G.; Schwenke, D. W. *J. Phys. Chem.* **1996**, *100*, 13588. (b) Lynch, G. C.; Truhlar, D. G.; Brown, F. B.; Zhao, J. G. *J. Phys. Chem.* **1995**, *99*, 207. (c) Truhlar, D. G.; Garrett, B. C.; Hipes, P. G.; Kuppermann, A. *J. Chem. Phys.* **1984**, *81*, 3542.

(49) For recent examples, see: (a) Corchado, J. C.; Truhlar, D. G.; Espinosa-García, J. *J. Chem. Phys.* **2000**, *112*, 9375. (b) Roberto-Neto, O.; Coitino, E. L.; Truhlar, D. G. *J. Phys. Chem. A* **1998**, *102*, 4568. (c) Liu, Y.; Lu, D.; Gonzalezlafont, A.; Truhlar, D. G.; Garrett, B. C. *J. Am. Chem. Soc.* **1993**, *115*, 7806.

(50) Brooks, B. R.; Burccoleri, R. E.; Olafson, B. D.; States, D. J.; Swaminathan, S.; Karplus, M. *J. Comput. Chem.* **1983**, *4*, 187.

(51) Fischer, S.; Karplus, M. *Chem. Phys. Lett.* **1992**, *194*, 252.

(52) Cui, Q.; Karplus, M. *J. Am. Chem. Soc.* **2002**, *124*, 3093.

(53) POLYRATE version 8.0; Chuang, Y.; Corchado, J. C.; Fast, P. L.; Villa, J.; Coitino, E. L.; Hu, W.; Liu, Y.; Lynch, G. C.; Nguyen, K.; Jackels, C. F.; Gu, M. Z.; Rossi, I.; Clayton, S.; Melissas, V.; Steckler, R.; Garrett, B. C.; Isaacson, A. D.; Truhlar, D. G. Department of Chemistry and Supercomputer Institute, University of Minnesota: Minneapolis, MN, 1998.

(54) Kim, Y.; Truhlar, D. G.; Keevoy, M. M. *J. Am. Chem. Soc.* **1991**, *113*, 7837.

(55) Swain, C. G.; Stivers, E. C.; Reuwer, J. F., Jr.; Schaad, L. J. *J. Am. Chem. Soc.* **1958**, *80*, 5885.

(56) (a) Goldanskii, V. I. *Dokl. Akad. Nauk SSSR* **1959**, *124*, 1261. (b) Goldanskii, V. I. *Dokl. Akad. Nauk SSSR* **1959**, *127*, 1037. (c) Häggi, P.; Grabert, H.; Ingold, G. L.; Weiss, U. *Phys. Rev. Lett.* **1985**, *55*, 761.

(57) Page, M.; McIver, J. W., Jr. *J. Chem. Phys.* **1988**, *88*, 922.

(58) Siebrand, W.; Smedarchina, Z.; Zgierski, M. Z.; Fernández-Ramos, *Int. Rev. Phys. Chem.* **1999**, *18*, 5.

(59) (a) Cui, Q.; Karplus, M. *J. Am. Chem. Soc.* **2001**, *123*, 2284. (b) Cui, Q.; Karplus, M. *J. Phys. Chem. B* **2002**, *106*, 1768.

(60) For some recent discussions, see, for example: (a) Jang, S.; Schwieters, C. D.; Voth, G. A. *J. Phys. Chem. A* **1999**, *103*, 9526. (b) Golosov, A. A.; Reichman, D. R. *J. Chem. Phys.* **2001**, *114*, 1065.

(61) Skodje, R. T.; Truhlar, D. G. *J. Phys. Chem.* **1981**, *85*, 624.

(62) (a) Borchert, T. V.; Abagyan, R.; Jaenicke, R.; Wierenga, R. K. *Proc. Natl. Acad. Sci. U.S.A.* **1994**, *91*, 1515. (b) Åqvist, J.; Fothergill, M. *J. Biol. Chem.* **1996**, *271*, 10010.

(63) For a recent review, see: *New Trends in Kramers' Reaction Rate Theory*, Talkener, P., Häggi, P., Eds.; Kluwer Academic: Dordrecht, The Netherlands, 1995.

(64) Neria, E.; Karplus, M. *Chem. Phys. Lett.* **1997**, *267*, 23.

(65) (a) Karplus, M. *J. Phys. Chem. B* **2000**, *104*, 11. (b) Berezhkovskii, A. M.; Szabo, A.; Weiss, G. H.; Zhou, H.-X. *J. Chem. Phys.* **1999**, *111*, 9952. (c) Doering, C. R.; Gadoua, J. C. *Phys. Rev. Lett.* **1992**, *69*, 2318.

(66) Neria, E.; Karplus, M. *J. Chem. Phys.* **1996**, *105*, 10812.

(67) Agarwal, P. K.; Billeter, S.; Ravi-Rajagopalan, P. T.; Benkovic, S. J.; Hammes-Schiffer, S. *Proc. Natl. Acad. Sci. U.S.A.* **2002**, *99*, 2794. (b) Agarwal, P. K.; Billeter, S.; Hammes-Schiffer, S. *J. Phys. Chem. B* **2002**, *106*, 3283.

(68) (a) Lakatos, S.; Halasz, G.; Zavodszky, P. *Biochem. Soc. Trans.* **1978**, *6*, 1195. (b) Vihinen, M. *Prot. Eng.* **1987**, *1*, 477.

(69) Kohen, A.; Klinman, J. P. *J. Am. Chem. Soc.* **2000**, *122*, 10738.

(70) Daniel, R. M.; Smith, J. C.; Ferrand, M.; Héry, S.; Dunn, R.; Finney, J. L. *Biophy J.* **1998**, *76*, 2504.